THE UNIVERSITY OF MICHIGAN

COLLEGE OF ENGINEERING
Department of Mechanical Engineering

Final Report

IMPROVED DISCONTINUITY DETECTION USING COMPUTER-AIDED ULTRASONIC PULSE-ECHO TECHNIQUES

Julian R. Frederick
James A. Seydel

ORA Project 360361

supported by:

WELDING RESEARCH COUNCIL
PRESSURE VESSEL RESEARCH COMMITTEE
MATERIALS DIVISION
SUBCOMMITTEE ON NONDESTRUCTIVE TESTING

administered through:

OFFICE OF RESEARCH ADMINISTRATION ANN ARBOR

December 1972

Eugen
UMK
1497

TABLE OF CONTENTS

LIST OF ILLUSTRATIONS

LIST OF ILLUSTRATIONS (Continued)

LIST OF ILLUSTRATIONS (Concluded)

ABSTRACT

The purpose of this project has been to investigate means for obtaining improved characterization of the size, shape, and location of subsurface discontinuities in metals. This has been done by applying computerized data processing techniques to the signal obtained in conventional ultrasonic pulse-echo systems. The principle benefits are improved signal-to-noise ratio, and resolution.

The received ultrasonic pulse from a discontinuity is combined with a reference function in order to preserve both the phase and amplitude of the received pulse. Processing is performed on the power spectrum of the resultant signal. The reference function is also used to compensate for some of the frequency-dependent scattering caused by the material microstructure. During data acquisition, analog signal averaging improves the signal-to-noise ratio (SNR). After data acquisition, a digital deconvolution procedure improves the transducer longitudinal resolution.

An analysis of a mathematical model of the combined ultrasonic and data processing system shows that the system provides an order of magnitude increase in the longitudinal resolution and a 37 dB increase in the signal-to-noise ratio over that expected from a conventional pulse-echo system. Experimental data demonstrate a factor of five improvement in resolution and a 28 dB increase in the SNR. The results also show that the computer processed data are virtually independent of the transducer used in the ultrasonic system. A theoretical analysis of the model also shows that the final output format is ideally suited to the formation of a synthetic transducer array designed to increase the lateral resolution.

Possible applications of this data processing system to current problems in nondestructive testing are discussed. The testing of materials with large amounts of internal scattering and frequency dependent attenuation appears to be particularly promising. Also, the enhanced resolution gained by the system can be used to reveal previously undetectable discontinuities in thin plates or those that are near a reflecting surface such as in immersion testing.

I. INTRODUCTION

OBJECTIVE

The objective of the investigation has been to develop an improved method for determining the size, shape, and location of a discontinuity using ultrasonic pulse-echo technique. This has been done by combining the echo from a discontinuity with a uniform reference echo, as is done in holography, and obtaining their combined power spectrum. The use of a reference echo preserves the phase and amplitude of the echo from the discontinuity. The use of a reference echo also compensates for some of the frequency-dependent scattering caused by the microstructure of the material. During data acquisition, analog signal averaging improves the signal-to-noise ratio (SNR). After data acquisition, a digital deconvolution procedure improves the transducer longitudinal resolution.

The final output format is ideally suited to the formation of a synthetic transducer array (using a single scanning transducer) which would provide increased lateral resolution. Improvements in SNR and longitudinal resolution have been demonstrated in the present investigation. The extension of the work to a synthetic array is a logical next step, but it has not been attempted in this investigation.

The results of the investigation show that the computer-processed data are virtually independent of the characteristics of the transducer used in the ultrasonic system. This is an important property when data taken over a period of years are to be analyzed for changes in the number and size of the discontinuities being monitored.

DECONVOLUTION

One of the problems in ultrasonic NDT is how to optimize trade-off between resolution and sensitivity. High resolution requires short-time pulses, and short-time pulses mean a reduced sensitivity. Sokolov (1941) proposed a frequency modulation technique which could circumvent this difficulty by forming pulses with a large time-bandwidth product, but the technique was superceded by the pulse-echo method and has never played an important role in subsequent developments.

When electronic pulses shorter than a microsecond are applied to a transducer, the output pulse shape is primarily determined by the high Q of the piezoelectric transducer. The transducer Q can be reduced by mechanical damping, but again this has a detrimental effect on sensitivity. Deconvolution of the transducer response is a possible answer to this problem that has been

thoroughly discussed in other related fields but never rigorously pursued in ultrasonics. Deconvolution will remove the relatively slow time response of the transducer, and while it normally reduces the system sensitivity by increasing the noise, sensitivity can be retained, and even increased, by signal averaging before the deconvolution step. Thus, more resolution and more sensitivity can be attained simultaneously by a sequence of signal averaging and deconvolution.

PLAN OF THE INVESTIGATION

An ultrasonic pulse-echo NDT system is proposed in which improved discontinuity characterization would be obtained by means of a high resolution, incremental transducer scan over the test surface at a position above the suspected discontinuity. The information returned by the target echoes at each point in this scan would be digitized and stored in a computer. The digital information from the complete collection of these discrete scanning points would be manipulated and processed into a form suitable for viewing the defect geometry on a CRT display.

Since resolution improvement is a key part of such a scanning system the present effort has been directed toward the development of a computer data processing system designed to improve both the longitudinal and lateral resolution. The data processing system divides logically into two parts: data acquisition and data processing. Due to the high frequencies involved, it is not possible to acquire data with the desired accuracy from the usual time representation of the ultrasonic echoes. However, sufficiently accurate data can be acquired from the power spectrum of the ultrasonic echoes, and a system designed to do this will be described and analyzed. Analog signal averaging is a necessary part of this data acquisition system, and it is implemented immediately before the actual analog-to-digital conversion.

Once the data are in digital form, the piezoelectric trnasducer response is deconvolved from the complete system response. This deconvolution procedure has a dual benefit. First, it improves the longitudinal resolution of the ultrasonic system. This is the primary goal. Second, it makes the output display imdependent of any long-term variations in transducer response due to aging or replacement. With the deconvolved data from many points stored in the computer, it can process the data to form an ultrasonic array designed to improve the lateral resolution. Thus, the data processing system can improve both the longitudinal and the lateral resolution.

Experimental evidence is presented to confirm the feasibility of longitudinal resolution enhancement, SNR improvement, and transducer independence. The possibility of an ultrasonic array derives naturally from the final form of the computer processed data, but no experimental data designed to show its feasibility are presented. The relationship of these three improvements to

both the proposed new scanning system and the conventional pulse-echo NDT system are discussed in detail.

II. THEORETICAL CONSIDERATIONS

MODEL OF AN ULTRASONIC NDT SYSTEM

A model for the pulse-echo ultrasonic system which has been developed is shown in Figure 1. Each box is a linear, time-invariant system that represents a particular process in the ultrasonic system. All impulse responses are shown as functions of time. In situations where distance is the natural independent variable, it is transformed into a time variable by the formula $t = d/v$. The pulser provides the input function, and the output function is the electrical signal representing the target echos. Each box is assigned an impulse response and a frequency response as indicated in Figure 1.

A digital data acquisition and processing system accurately samples and processes the output of the model. This system consists of a wave analyzer, a low-pass filter, an analog-to-digital converter, a digital deconvolution, and an inverse Fourier transform. After the data are digitized, the model of the ultrasonic system is enlarged to include the digital data acquisition processing system, and again the response of this larger model to an arbitrary input and to band-limited Gaussian noise is determined. A complete theoretical development and justification of the model has been developed by Seydel (Seydel, 1972).

The model is presented in this manner in order to emphasize the fact that a conventional ultrasonic system measures the reflectivity function, $g(t)$, only after it passes through a piezoelectric transducer that modifies and distorts the signal. For example, Figure 2 shows that in a conventional system, a single discontinuity (the back surface) is represented by a different indication for each different transducer. As the following analysis demonstrates, these transducer-induced modifications can be removed, and the reflectivity function can be directly measured.

ANALYSIS OF THE MODEL

The system output function is now derived using the following results from linear systems theory (Kaplan, 1962).

1. The system output is equal to the convolution of the system input with the system impulse response. The convolution of the two functions $a(t)$ and $b(t)$ is denoted by $a(t) * b(t)$ and is defined to be the following:

$$a(t) * b(t) = \int_{-\infty}^{\infty} a(t')\, b(t-t')dt' \qquad (1)$$

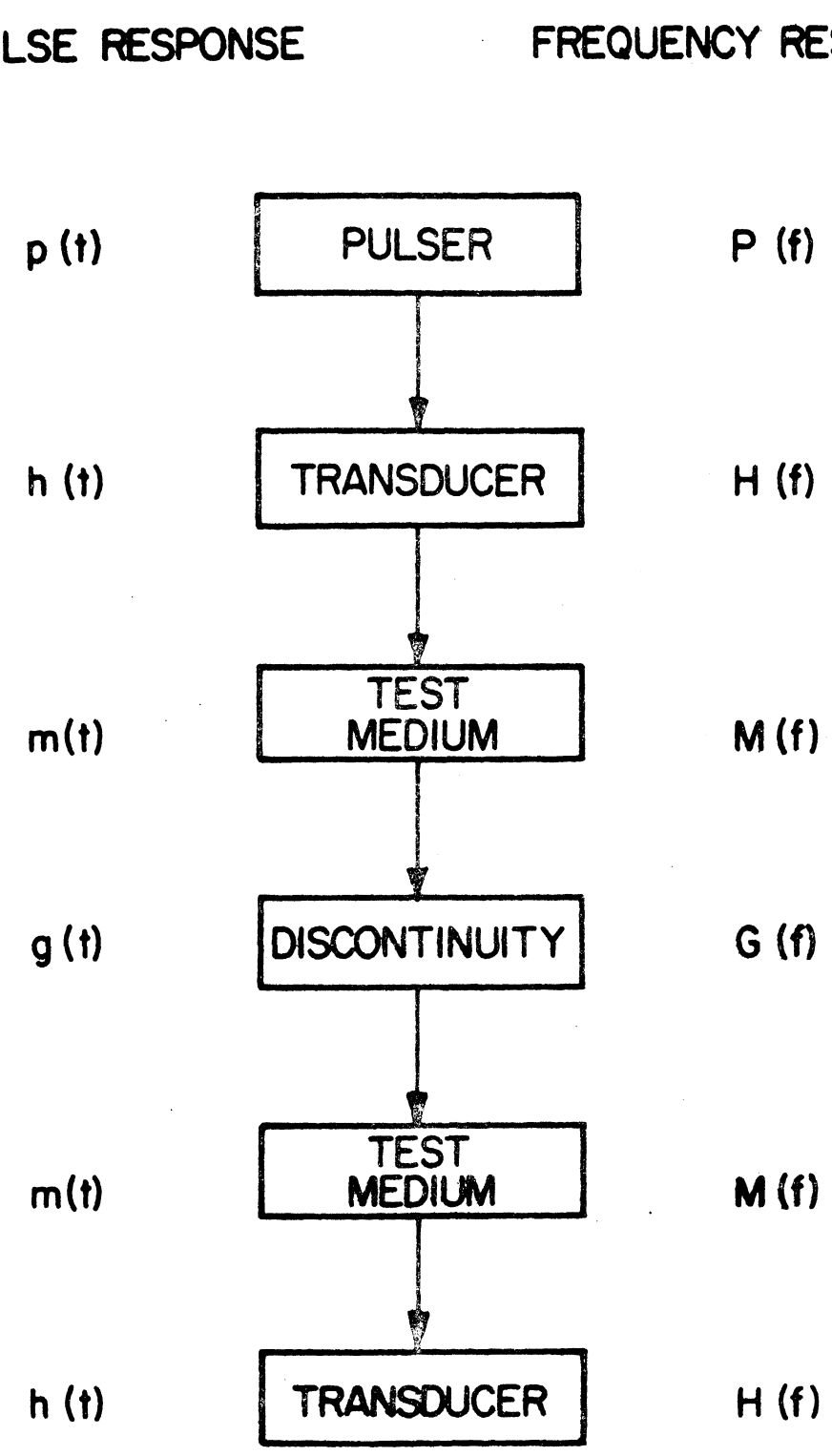

Figure 1. Mathematical model of a pulse-echo ultrasonic nondestructive testing system. Each physical function is represented by a linear, time-invariant system.

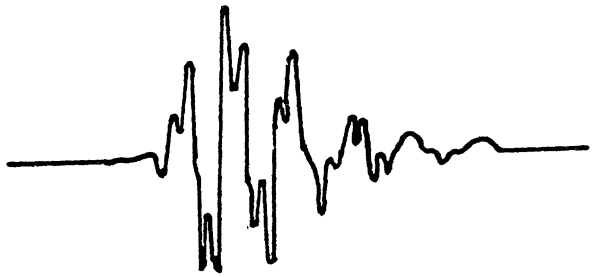

2a. 2.25 MHz, 13-mm diameter transducer.

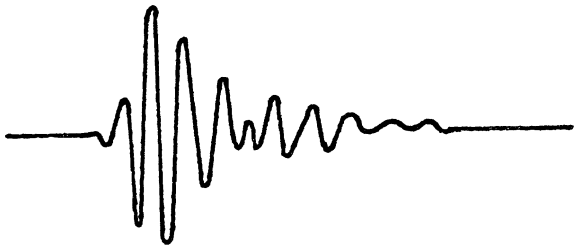

2b. 10 MHz, 6.4-mm diameter transducer.

2c. 5 MHz, 13 mm-diameter transducer.

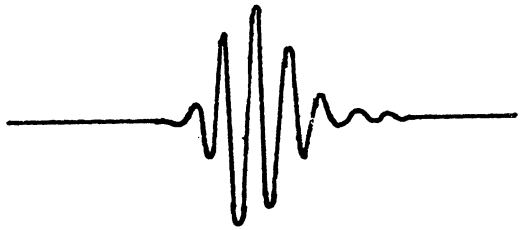

2d. 10 MHz, 6.4-mm diameter transducer.

Figure 2. Loop impulse response of four different transducers. Time scale in 2a is compressed by a factor of 2.5 compared to the other figures.

2. The output frequency response is equal to the input frequency response multiplied by the system frequency response.

3. The system impulse response and the system frequency response are a Fourier transform pair. The Fourier transform of a lower case time function, a(t), will be denoted by an upper case frequency function, A(f), where f is the frequency.

Using the first property, the output, f(t), of the ultrasonic system is written as

$$f(t) = n(t) * m(t) * g(t) * m(t) * h(t) \tag{2}$$

or using properties 2 and 3,

$$F(f) = H^2(f)\, M^2(f)\, G(f) \tag{3}$$

Equations (2) and (3) describe the cumulative effect of the transducer, the media, and the discontinuity upon the final output.

Given F(f), each of the terms in equation (3) can be measured by properly arranging the experimental conditions. For instance, H(f) can be found by insonifying only a single-point target in a medium with no frequency-dependent attenuation. In this case, G(f) = 1, M(f) = 1, and $F(f) = H^2(f)$. This result can then be used to find M(f) by insonifying a single-point target in a medium with frequency-dependent attenuation. Then $F(f) = H^2(f)\, M^2(f)$ and M(f) is found by dividing this formula by the previously measured $H^2(f)$. As mentioned earlier, measuring G(f) directly is one of the major goals of this research effort, and a method for accomplishing this task is presented below.

It must be emphasized that H(f) and M(f) are not constant properties of any particular transducer or medium. Since the coupling conditions between the transducer and the medium have been implicitly included in the transducer response, H(f) can be different for the same transducer in contact with different media. Also, M(f) is a function of the distance of travel of the acoustic pulse. This fact becomes important in subsequent derivations when a different form of M(f) must be assigned to the defect and reference functions, respectively.

Measurement of H(f) and M(f) is complicated by the fact that, in most cases, F(f) is not directly measurable. Almost all spectrum analyzers (including all high-frequency spectrum analyzers) measure the power spectrum, S(f), where $S(f) = F(f)\, F^+(f)$ and $F^+(f)$ is the complex conjugate of F(f). A method circumventing this difficulty is considered below.

The output of the ultrasonic system, f(t), is primarily determined by the transducer loop response, h(t) * h(t). If this function is applied to the input of a spectrum analyzer, the output if $[H(f)\ H^{+}(f)]^2$. A graph of $[H(f)\ H^{+}(f)]^2$ for a high resolution, 5 MHz transducer is shown in Figure 3. The ordinate in this figure is approximately logarithmic. Figure 3 demonstrates that the 5 MHz transducer produces power not only at its center frequency but also in a band of frequencies ranging from about 2 MHz to 8 MHz.

DATA ACQUISITION AND PROCESSING

At this point, it is necessary to consider some characteristics of the digital system that processes f(t). The most important part of the digital system is the analog-to-digital converter (ADC) that transforms the analog waveform into a set of digital data. The electrical characteristics of the ADC are largely determined by the upper frequency limit of f(t). The curve shown in Figure 3 will be considered as the typical frequency response of an ultrasonic transducer. In evaluating the ADC, both the time and amplitude accuracy are specified as 8 bits. The reason for this tight specification is made clear later.

An ADC contains two basic systems: a sample-and-hold amplifier preceding an analog-to-digital encoder. The sample-and-hold module is necessary because most high-speed encoders require a constant input signal during the conversion period. The sample-and-hold module is characterized by two time constants: the acquisition time and the aperture time. The acquisition time is defined as the time required for the output to go from its most negative condition to its most positive condition. The acquisition time represents the maximum time for the output to reacquire and to track the input. The aperture time is defined as the time bracket within which the output stops tracking and holds the input voltage. The actual sampling time within this bracket is a random process. The analog-to-digital encoder is characterized by the time required to produce a digital representation of the input signal to the necessary accuracy (usually stated in bits). More accuracy typically implies a longer conversion time.

The ADC is operated by sending a timing pulse to the "sample" input of the sample-and-hold module. After the acquisition time has elapsed and the output is tracking the input to within the required accuracy, a timing pulse is sent to the "hold" input. The sample-and-hold module then holds this voltage while the digital encoder is activated, and, after the full conversion time has elapsed, a digital sample is available for storage. The complete process is reinitiated by a timing pulse to the "sample" input.

There are two possible techniques for using an ADC to digitize f(t). The first technique uses what is referred to as a free-running ADC to completely digitize f(t) during one operation of the pulser unit. The free-running ADC

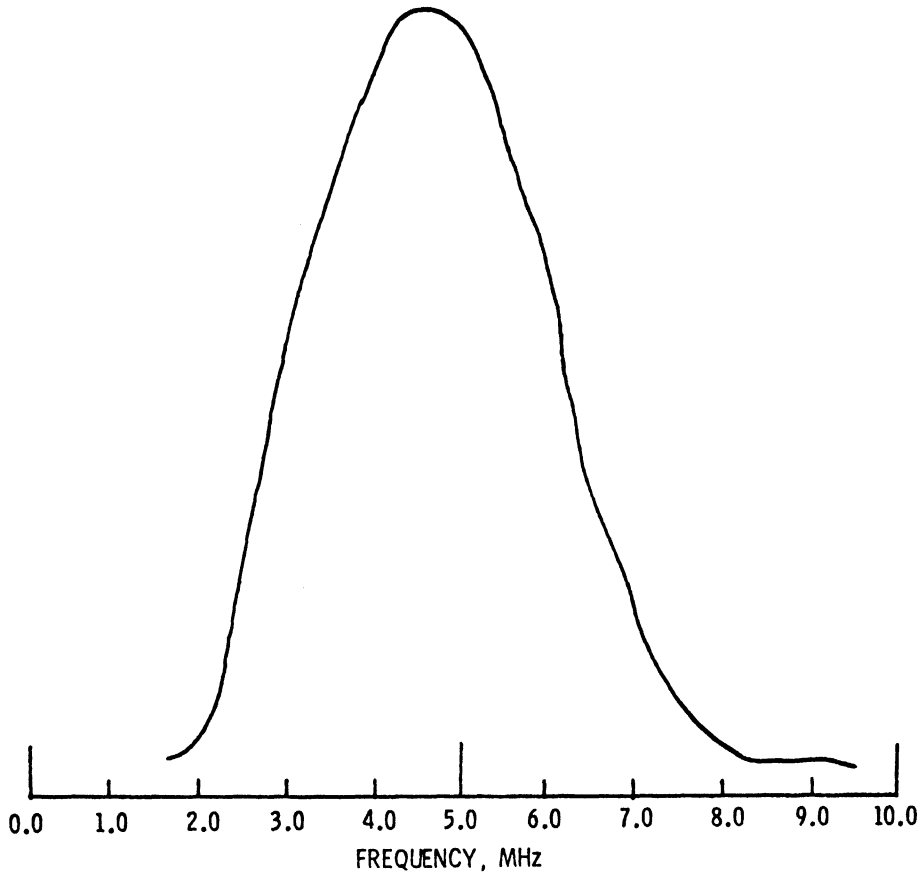

Figure 3. Power spectrum of the 5-MHz transducer in Figure 2c. The ordinate is approximately logarithmic.

samples and digitizes the waveform under the control of a high-frequency clock. During each clock pulse, a portion of the analog waveform is sampled, digitally encoded, and stored. Since the typical analog waveform has an upper frequency limit of 8 MHz, the clock frequency must be at least 16 MHz in order to satisfy the Nyquist criterion. To meet the specification of 8-bit accuracy for time and for amplitude at a 16-MHz clock frequency implies an aperture time of 0.5 ns, an acquisition time of 30 ns, and an 8-bit conversion time of 30 ns. Every one of these figures is from one to two orders of magnitude beyond the present state-of-the-art.

The second technique uses the fact that f(t) is a repetitive waveform. Under these conditions, the ADC can be programmed to slide the sample-and-hold aperture over f(t) while taking only one digital sample per pulse. Since the ultrasonic PRF is about 1 kHz, both the acquisition time and the conversion time can now be increased to around 0.5 ms, and these figures are well within the state-of-the-art. Unfortunately, the necessary aperture time is still 0.5 ns, and this figure is about two orders of magnitude beyond presently available instruments. If new technology can reduce the aperture time to 0.5 ns or less, this sampling technique would become a very attractive method of data acquisition.

Since neither method of directly digitizing f(t) is feasible, it is necessary to consider a novel approach to this problem. This new method employs a system that acquires the necessary data from the power spectrum of f(t) by using a wave analyzer. This approach has several advantages. There are many commercially available wave analyzers that make use of recent advances in phase-locked loops (PLL). A PLL allows the wave analyzer input frequency to be tuned with a stability and accuracy determined only by the stability of a single reference oscillator, even though there may be as many as three of four different local oscillators in the instrument. Since this same reference oscillator can be used to control the ultrasonic PRF, the wave analyzer can be servolocked to the ultrasonic system to provide drift-free spectral measurements. With a reference oscillator stability of 1 part in 10^6 per day and drift-free amplitude measurements, it is very easy to meet the 8-bit specification on frequency and amplitude accuracy. The excellent frequency stability also makes it possible to use a 200-Hz input bandwidth even when measuring 20-MHz signals. Such a narrow bandwidth is very important in reducing the omnipresent noise. The narrow bandwidth also imposes a relatively long settling time that is advantageous for inexpensive data conversion and storage.

The Fourier transform of a pulsed signal can be represented by a comb function whose amplitude envelope is the Fourier transform of a single pulse. For signals of infinite duration, this is equivalent to the Fourier series representation of f(t). The comb spacing is equal to the ultrasonic pulse rate frequency. Spectral measurements are made by tuning the wave analyzer to one of these comb spikes and measuring the power. The power readings are converted into a digital form by measuring the detector voltage with a digital voltmeter. This process is repeated for each comb spike.

The power spectrum has the singular disadvantage of not preserving the phase information present in f(t). If $F^+(f)$ is the complex conjugate of the Fourier transform of f(t), then the power spectrum of f(t) is denoted by $F(f)\ F^+(f)$, and the wave analyzer output is

$$F(f)\ F^+(f) = [|F(f)|e^{i\phi(f)}]\ [|F(f)|e^{-i\phi(f)}] = |F(f)|^2 \qquad (4)$$

All the phase information contained in $\phi(f)$ is no longer present at the output. Unless stated otherwise, it will be assumed that all physical outputs are complex-valued functions of a real variable (time or frequency).

The phase information in F(f) can be preserved by adding a reference function to f(t) prior to its insertion into the wave analyzer. The manner in which the phase information is preserved is shown by the example below. If a delta function is added to the normal ultrasonic system output, the final output is $f(t) + \delta(t)$. The Fourier transform of this output is $F(f) + 1$, and its power spectrum is $|F(f)|^2 + 1 + F^+(f) + F(f)$. If the various terms in this sum can be separated in some manner, then F(f) can be recovered with both phase and amplitude information intact. It is important to note that recovering F(f) is equivalent to recovering f(t) since they are uniquely related by a Fourier transform.

The particular phase reference function used can be chosen as a matter of convenience. If an arbitrary reference function, r(t), is used, then F(f) is multiplied by $R^+(f)$. In the example above, this modification would be undesirable because F(f) alone is required and no more processing is contemplated. But if additional processing is desirable, then r(t) can be chosen so as to simplify the subsequent systems. For example, in the deconvolution system described below, r(t) is chosen so that the deconvolution filter is an amplitude only filter. Since such a deconvolution filter has no phase reversals or axis crossings to complicate matters, this choice of r(t) results in a considerable simplification.

ANALYSIS OF THE DATA PROCESSING SYSTEM

Since the high Q impulse response of the piezoelectric transducer is primarily responsible for the slow time response of the ultrasonic system, a deconvolution system that compensates for the transducer impulse response, h(t), is very attractive. This is accomplished in the following manner. Assume that an arbitrary stress function, a(t), is applied to the transducer input, and that the transducer output voltage is b(t). Then

$$b(t) = \int_{-\infty}^{\infty} a(t')\ h(t-t')dt' \qquad (5)$$

Since h(t) can be measured, and b(t) is known, this integral equation can be solved for a(t). A formal solution to the deconvolution problem is quickly achieved by taking the Fourier transform of both sides of the convolution integral. Then $B(f) = A(f)\ H(f)$ and $A(f) = B(f)/H(f)$. Now, a(t) is found by taking the inverse Fourier transform of A(f). If H'(f) is defined as 1/H(f), then $A(f) = B(f)\ H'(f)$ and the deconvolution process becomes an additional linear system whose input is b(t) and whose output is a(t). Since the frequency response of the deconvolution process is the inverse of the transducer frequency response, the deconvolution process is frequently called the "inverse filter" for h(t), in an analogy with electrical filters.

The application of a digital deconvolution procedure to the complete ultrasonic system is a fairly simple matter since the data acquisition system described above already provides digital spectral data. The first step in forming the inverse filter is to measure h(t) and b(t), or equivalently H(f) and B(f). This process is illustrated by computing the output of the ultrasonic system when two different types of target reflectivity functions are assumed.

Example 1. Assume that the target is a point reflector located a time T away from the transducer. Then $g(t) = \delta(t-T)$ and the output, $f_1(t)$, is

$$\begin{aligned} f_1(t) &= h(t) * m(t) * \delta(t-T) * m(t) * h(t) \\ &= h(t) * m(t) * m(t-T) * h(t) \end{aligned} \tag{6}$$

The Fourier transform of $f_1(t)$ is

$$F_1(f) = H^2(f)\ M^2(f)\ e^{-i\,2\pi f T} \tag{7}$$

and the power spectrum, S(f), of $f_1(t)$ is

$$S_1(f) = [H(f)\ H^+(f)]^2\ [M(f)\ M^+(f)]^2 \tag{8}$$

Example 2. Assume that g(t) is any arbitrary reflectivity function localized in an area where the media response is denoted by $m_1(t)$, and that a reference function is derived from a point target located a time T from the transducer. Then

$$f_2(t) = [h(t) * m_1(t) * g(t) * m_1(t) * h(t)]$$

$$+ [h(t) * m(t) * m(t-T) * h(t)] \tag{9}$$

and

$$F_2(f) = H^2(f)\, M_1^2(f)\, G(f) + H^2(f)\, M^2(f)\, e^{-i 2\pi f T}$$

$$= H^2(f)\, M^2(f) \left[\frac{M_1^2(f)}{M^2(f)}\, G(f) + e^{-i 2\pi f T} \right]$$

$$= H^2(f)\, M^2(f) \left[M_2(f)\, G(f) + e^{-i 2\pi f T} \right] \tag{10}$$

where

$$M_2(f) = \frac{M_1^2(f)}{M^2(f)} \tag{11}$$

and the power spectrum $S_2(f)$ is

$$S_2(f) = [H(f)\, H^+(f)]^2\, [M(f)\, M^+(f)]^2$$

$$\left[M_2(f)\, M_2^+(f)\, G(f)\, G^+(f) + 1 + e^{-i 2\pi f T} \right.$$

$$\left. G^+(f)\, M_2^+(f) + e^{i 2\pi f T}\, G(f)\, M_2(f) \right] \tag{12}$$

The deconvolution procedure now becomes obvious. The first two bracketed terms in $S_2(f)$ are exactly equal to $S_1(f)$. Thus

$$S_2(f) = S_1(f) \left[M_2(f)\, M_2^+(f)\, G(f)\, G^+(f) + 1 + e^{-i 2\pi f T} \right.$$

$$\left. G^+(f)\, M_2^+(f) + e^{i 2\pi f T}\, M_2(f)\, G(f) \right] \tag{13}$$

For the moment, consider the case where the scattering due to the medium is negligible at all points within the test block. Thus $M(f) = M_1(f) = M_2(f) = 1$. A thorough treatment of the effects of the medium will be postponed until Section V. Then by defining $S(f) = S_2(f)/S_1(f)$

$$S(f) = G(f)\,G^{+}(f) + 1 + e^{-i\,2\pi f T}\,G^{+}(f) + e^{i\,2\pi f T}\,G(f) \qquad (14)$$

and taking the inverse Fourier transform of S(f) gives

$$s(t) = g'(t) + g(-t+T) + g(t-T) \qquad (15)$$

where g'(t) is the inverse Fourier transform of [G(f) G^{+}(f) + 1]. Equation (15) presents the form of the output from the complete ultrasonic and data processing system. As promised, it is a direct measure of the reflectivity function, including both the phase and the amplitude.

First, it is necessary to establish that g(t) can be separated from the other terms in s(t). Since g(t) is generally localized in a small region of the t-axis, let this region be delimited by two delta functions, $\delta(t-T_1)$ and $\delta(t-T_2)$. Then

$$S(f) = 3 + e^{-i\,2\pi f(T_1-T_2)} + e^{i\,2\pi f(T_1-T_2)} + e^{i\,2\pi f(T_1-T)} + e^{i\,2\pi f(T_2-T)} + e^{-i\,2\pi f(T_1-T)} + e^{-i\,2\pi f(T_2-T)} \qquad (16)$$

and

$$s(t) = 3\delta(t) + \delta(t-T_1+T_2) + \delta(t+T_1-T_2) + \delta(t+T_1-T) + \delta(t+T_2-T) + \delta(t-T_1+T) + \delta(t-T_2+T) \qquad (17)$$

The second and third terms in s(t) are referred to as the cross products, and the fourth through seventh terms are g(t) and its reflection through the t = 0 axis. The reference function can come either before or after the target g(t). If the reference function comes after the targets, as shown in Figure 4a, then s(t) is as graphed in Figure 4b. This is the case for all the data presented in Section IV. Since S(f) is real, s(t) is symmetrical about the t = 0 axis, and it is graphed only for t > 0. As can be seen from Figure 4b, g(t) can be separated from the cross product terms in s(t) if $T - T_2 > T_2 - T_1$. Since T_2 is the point in g(t) nearest to the reference function, this condition implies that the duration from T_2 to the reference function must be greater than the duration of g(t). A similar analysis using Figures 4c and 4d when the reference function precedes g(t) again reveals that the duration from the closest point in g(t) to the reference function must be greater than the duration of g(t) in order that the various terms in s(t) may be separated.

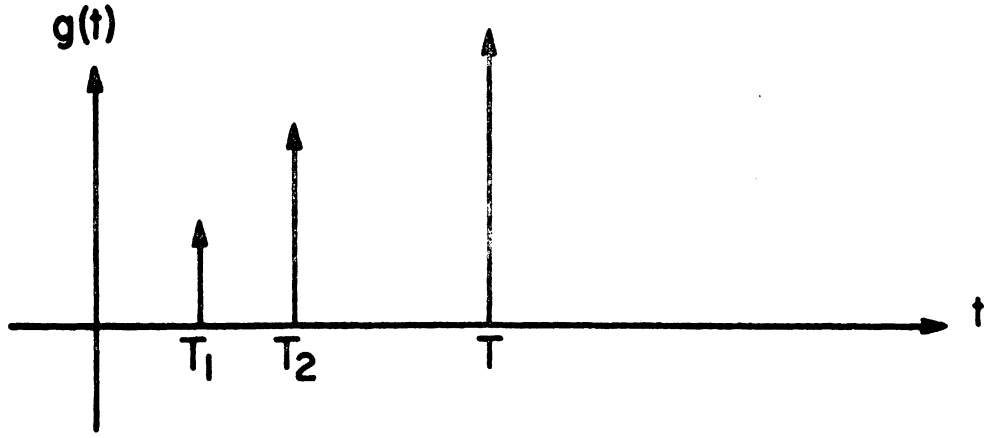

Figure 4a. Graph of a discontinuity delimited by $\delta(t-T_1)$ and $\delta(t-T_2)$. The reference function, $\delta(t-T)$, follows the discontinuity.

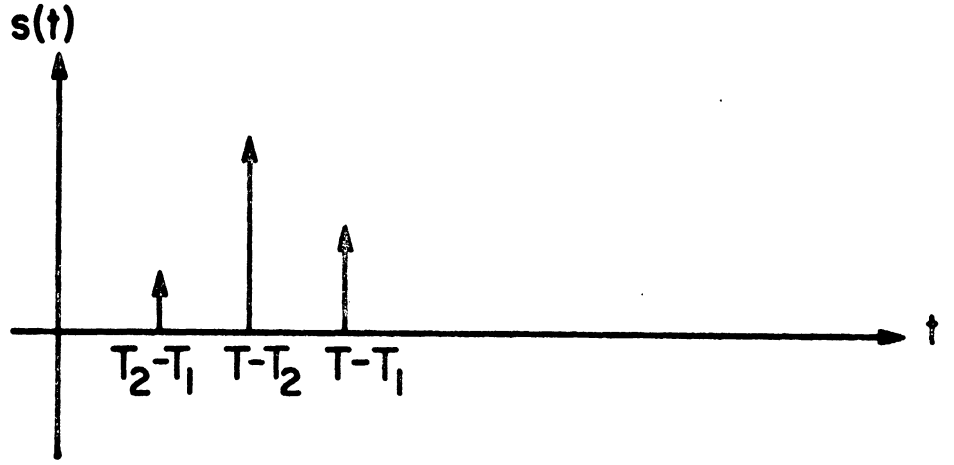

Figure 4b. Graph of $s(t)$ as derived from the $g(t)$ in Figure 4a. $\delta(t-T_2+T_1)$ is a cross product term and the discontinuity is delimited by $\delta(t-T+T_2)$ and $\delta(t-T+T_1)$. Note that the time reversal changes in the order of the two delimiters.

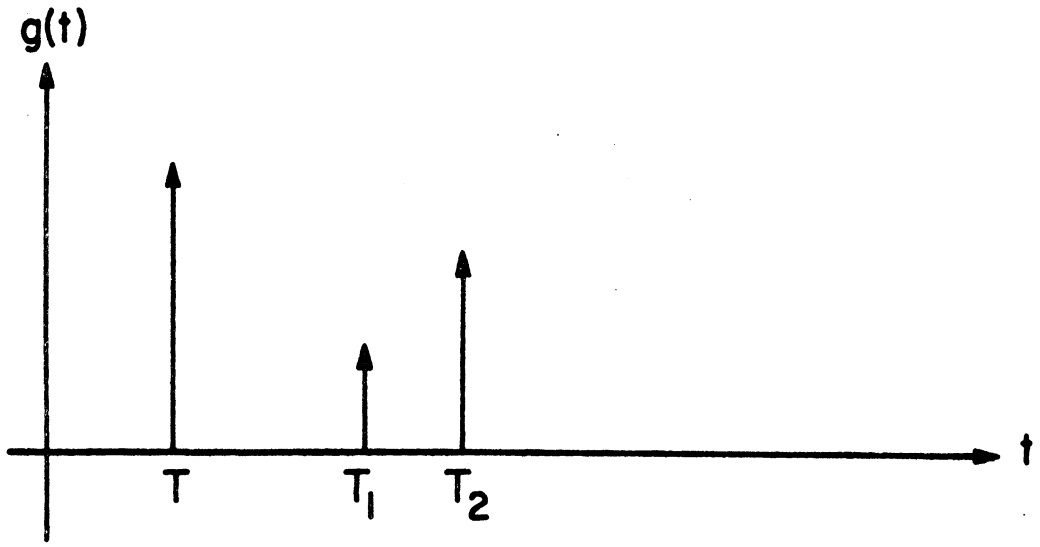

Figure 4c. Graph of a discontinuity delimited by $\delta(t-T_1)$ and $\delta(t-T_2)$. The reference function, $\delta(t-T)$, precedes the discontinuity.

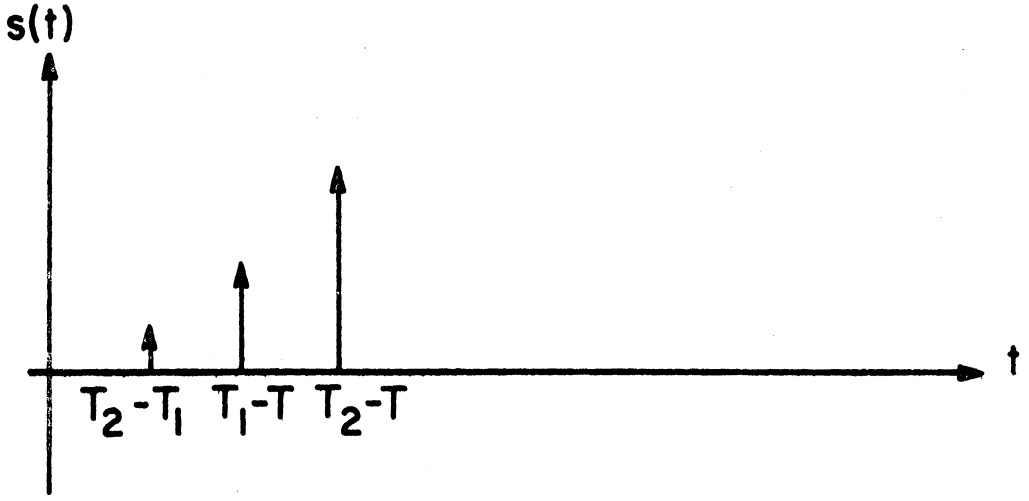

Figure 4d. Graph of s(t) as derived from the g(t) in Figure 4c. $\delta(t-T_2+T_1)$ is a cross product term and the discontinuity is delimited by $\delta(t-T_1+T)$ and $\delta(t-T_2+T)$. Note that there is no time reversal.

Figure 16 in Section III shows a situation where g(t) is not separated from the cross product terms. Figure 16a shows two large targets delimiting some smaller targets and followed by the reference function. In this example $T - T_2 < T_2 - T_1$. The deconvolved data shown in Section IV in Figure 16b reveal two false targets, a and b, that are the cross products between target c and targets d and e. Targets c, d, and e and everything in between are all true indications.

The Fourier inversion step referred to above is a digital Fourier transform (DFT) implemented on a digital computer using the recently developed fast Fourier transform (FFT) technique. Thus the DFT of a time sequence, f(nT), is denoted by F(kΩ) and

$$F(k\Omega) = \sum_{m=0}^{M-1} f(nT)\, e^{-i\Omega nkT} \tag{18}$$

and

$$f(nT) = \frac{1}{N} \sum_{k=0}^{N-1} F(k\Omega)\, e^{i\Omega nkT} \tag{19}$$

where $\Omega = 2\pi/NT$ and T is the uniform sampling interval in the time domain. Gold and Rader (1969, page 162) show that M = N, that is, the number of discrete frequency samples generated by a DFT is equal to the number of discrete time samples. They also show that

$$DFT(e^{i\Omega qnT}) = N\delta_{kq} \tag{20}$$

Thus, the DFT has the same frequency selective properties as the normal Fourier transform. The factor of N appearing on the right side of equation (20) distinguishes the DFT from the conventional Fourier transform (FT) since

$$FT\left(e^{i\,2\pi f_o t}\right) = \delta(2\pi f - 2\pi f_o) \tag{21}$$

Thus all power terms which are derived from a function processed by a DFT will be a factor of N^2 greater than those processed by a conventional Fourier transform.

SIGNAL-TO-NOISE RATIO ANALYSIS

Up to now, all the signals in the ultrasonic and data processing systems have been assumed to be completely deterministic. This assumption is now

discarded in order to derive a formula expressing the SNR of the combined ultrasonic and data processing system in terms of the SNR of a conventional ultrasonic system.

There are two important noise sources in an ultrasonic system: reflections from the randomly distributed grain structure and thermal noise in the ultrasonic transducer. Since the target is usually much larger than the grain structure of the medium, the random fluctuations in output in the vicinity of a target are negligible. Thus primarily, the random acoustic reflections scatter the acoustic energy out of the main lobe of the transducer radiation pattern and reduce the output voltage of the transducer. Therefore, the following analysis assumes that the thermal noise is the primary noise source. As Davenport and Root (1958, page 185) state, thermal noise can be represented by a Gaussian process with a flat power spectrum.

The SNR for a conventional ultrasonic system is considered first. This system is modeled in Figure 5a. From the model it can be shown (Seydel, 1972, page 47) that the signal-to-noise ratio for the unprocessed data is

$$(SNR)_u = \frac{1/2 \sum_m A_m^2}{2N_o B_o}$$

where N_o is the spectral density of the noise, B_o is the bandwidth of the filter, P(f), and the numerator is signal power.

The model of the ultrasonic and data processing system is shown in Figure 5b. The wave analyzer is modeled as a tunable bandpass filter, K(f), followed by a square law device and a low pass filter, L(f). After the bandpass filter is tuned over the bandwidth of the ultrasonic signal, the resulting ensemble of frequency samples is Fourier transformed to yield the final output. The deconvolution filter is omitted from this analysis as its effect will be considered below.

An analysis of the model (Seydel, 1972, page 47) shows that the SNR of the processed data, $(SNR)_p$, is

$$(SNR)_p = \left[\frac{(SNR)_u^2}{2(SNR)_u + \frac{B_1}{MB_o}}\right]\left[\frac{B_o}{B_1 + B_2}\right] \qquad (22)$$

where B_o is the bandwidth of the ultrasonic transducer, B_1 is the bandwidth of the wave analyzer, IF filter, B_2 is the bandwidth of the low-pass filter, and M is the number of samples taken from the power spectrum.

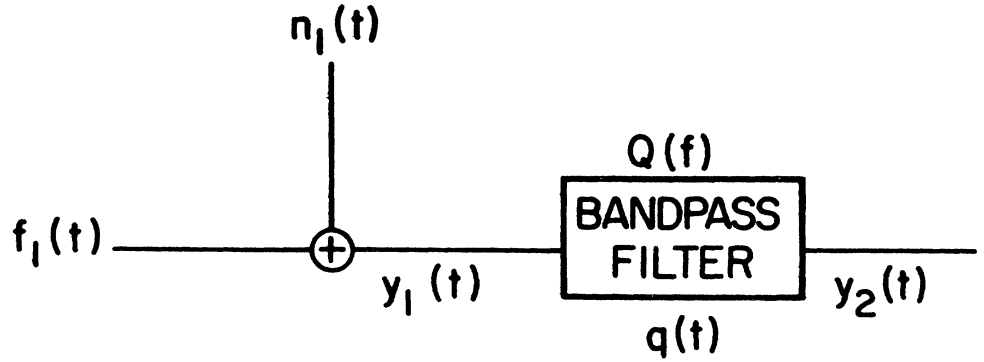

Figure 5a. Model of a conventional pulse-echo ultrasonic system with output $f_1(t)$ combined with additive noise $n_1(t)$ and inserted into a rectangular bandpass filter Q(f) designed to optimize the SNR.

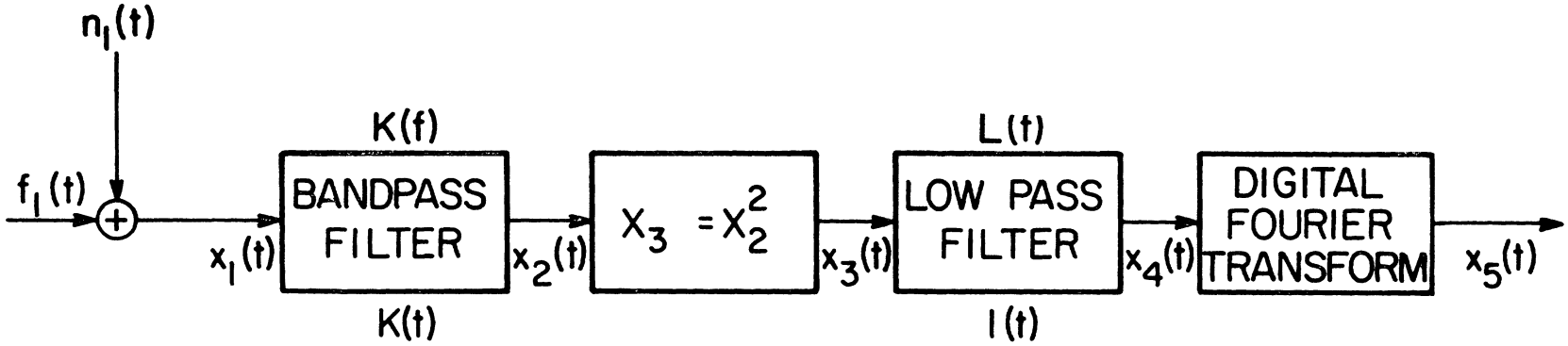

Figure 5b. Model of the data processing system. The output from the ultrasonic system, $f_1(t)$, is combined with additive noise, $n_1(t)$, to form $x_1(t)$.

Equation (23) is the formula relating the SNR of the data processing system to the SNR for the conventional ultrasonic system. This formula can be simplified slightly by considering some typical numbers for the various parameters. In the experimental work presented below, the following values for M, B_o, B_1, and B_2 are typical.

$$M = 256 \qquad B_o = 2.0 \text{ MHz} \qquad B_1 = 200 \text{ Hz} \qquad B_2 = 1 \text{ Hz} \tag{24}$$

Then

$$\frac{B_1}{MB_o} < 10^{-6} \tag{25}$$

and this term will be considered negligible. Thus

$$\frac{(SNR)_p}{(SNR)_u} = \frac{B_o}{2(B_1 + B_2)} \cong \frac{B_o}{2B_1} = 5000 \tag{26}$$

and the data processing system introduces a 37 dB increase in the SNR.

Note that both M and B_2 appear to have very little effect on the final SNR. This is not true. If B_2 is not explicitly provided as a filter external to the wave analyzer, it still has to be included as the low pass filter inside the wave analyzer which normally follows the square law device. In a typical high frequency wave analyzer, B_2 is about 10 kHz, but without another noise source, any B_2 which is greater than 200 Hz only decreases the SNR by 3 dB. In fact, the amplifiers in the wave analyzer introduce a noise source not included in the above analysis. In this case, both M and B_2 increase the SNR more than shown in equation (23). The narrow bandwidth of B_2 averages the voltage over time, and the factor of M is due to the Fourier transform providing a weighted average over the ensemble of power samples.

The formal mathematics tends to obscure the physical basis of this increase in SNR. It is merely due to the fact that the ultrasonic system is a pulsed, evoked response system. In such a system, the pulsed signal always occurs at the same point in time while the noise at this point in time fluctuates in value for each succeeding pulse. If for a given point in time, the voltage produced by each pulse is added onto the voltage produced by the previous pulse, then the signal voltage is cumulative while the noise voltage fluctuates and eventually cancels out. In the data processing system, the narrow bandwidths of B_1 and B_2 provide this additive or averaging effect.

INTERPRETATION OF THE ANALYSIS

As equation (15) demonstrates, the output of a data processing system consisting of a wave analyzer, an analog-to-digital converter, a digital deconvolution filter, and a Fourier transformer contains the reflectivity function, $g(t)$, in a form that can be easily recovered by a time-gating process. An output that is a direct measure of the reflectivity function has many advantages over a conventional ultrasonic system where the reflectivity function is modified by the transducer. These advantages, as well as some other responses characteristic of this form of the output, are discussed below.

Perhaps the most obvious advantage of measuring the reflectivity directly is that the format of the output is independent of the particular transducer used in the pulse-echo system. That is, a single point target is always displayed as a single spike at the output regardless of which transducer is used in the ultrasonic system. In a conventional system, a single point target is displayed in a wide variety of forms. This statement concerning transducer independence can be made even stronger if the transducer bandwidth is taken into consideration. For a collection of transducers of approximately equal bandwidth, not only is the output format the same, but the output function representing a complex target is virtually identical for each transducer.

Transducer independent output is important when test results taken over a period of years are compared for possible changes in flaw structure. Over this period of time, the piezoelectric crystal can age (Mason, 1950, page 100) or be replaced due to failure. Thus, in a conventional system, the flaw structure could appear to be modified when, in fact, the modification was strictly due to a change in transducer response. The data processing system output is not susceptible to this problem.

To a certain extent, this transducer independent output format is achieved in a conventional pulse-echo system by the rectification and low-pass filtering of the pulse before it is displayed. But this process suffers in comparison with the present data processing system because it achieves transducer independence at the expense of decreased resolution.

Another advantage is the increased resolving power provided by the data processing system. The impulse response of an ultrasonic transducer can be nicely approximated by an exponentially damped sinusoidal wave. With this assumption, plus the fact that accurate spectral measurements can be made at frequencies where the power is 20 dB below the power at the transducer center frequency, it is easy to show that the bandwidth of the deconvolved data is ten times the bandwidth of the unprocessed data. Since the bandwidth is directly proportional to the resolving power, the data processing system would have ten times the resolving power of the conventional ultrasonic system. In practice, the increase in resolving power for the processed data is usually between a factor of four and a factor of six.

Cox and Renken (1970) have considered the application of a deconvolution technique to electromagnetic transducers. They feel that the technique is not practical because the deconvolution filter is nonrealizable, amplifies small impulsive disturbances at the input, and reduces the SNR to zero. The deconvolution filter is nonrealizable only when implemented in the time domain. If the filter is constructed in the frequency domain as described above, no realizability problems are presented. Their second objection is really just a restatement of the third. Since the deconvolution filter is preceded by a transducer that smooths out any impulses applied to its input, the only possible source of such impulses is the transducer noise. But as was shown in the above section on system noise, the SNR at the deconvolution filter input is very high, even for a low SNR at the transducer. In order to calculate the SNR loss due to the deconvolution filter, it is necessary to know the explicit functional form of the transducer response. Thus it is not possible to make any general statements concerning the SNR at the deconvolution filter output. From the fact that experimental SNR improvement factors within 10 dB of the theoretical value have been achieved, it is believed that the SNR at the output of the deconvolution filter approximates the value predicted by equation (23) and represents a significant increase over what is expected from a conventional system.

While the data processing system output has both an improved resolving power and an improved SNR with respect to a conventional system, the usual trade-off between resolving power and SNR still exists. But now, the conflict has been escalated to a higher level. Figure 17 in Section IV is an example where errors in the deconvolution filter have decreased the SNR. Figure 10 is the same transducer located in a slightly different position with a properly constructed deconvolution filter. The resolution in Figure 17 is slightly better, but the SNR is badly degraded. This indicates that the resolution-SNR trade-off for the data processing system may be more severe than for the conventional system.

Equation (15) also demonstrates that both the phase and the amplitude of $g(t)$ have been preserved. This opens up the possibility of forming a synthetic array by taking data from many different transducer positions, processing the data into a form described by equation (15), and then summing the data with the appropriate phase. This technique would provide an extremely flexible display method since the array could be focused and directed under computer control after all the data has been collected. Thus, the computer processed data is in an extremely advantageous form for processing the data returned from the scanning system proposed in Section I.

III. EXPERIMENTAL PROCEDURE

EQUIPMENT

A schematic diagram of the complete ultrasonic and data processing system is shown in Figure 6.

From an experimental point of view, the most important element in Figure 6 is the 1-MHz reference oscillator. This oscillator links the wave analyzer, the pulser, and the range gates into a servo loop, and this servo loop provides the stability that enables highly accurate, drift-free measurements to be made on the ultrasonic data.

The reference oscillator provides a stable reference frequency (1 part in 10^6) for use within the three phase locked loops (PLL) contained within the analyzer and also, through the divider and timing circuits, triggers the ultrasonic pulser. Since the ultrasonic signal can be written as a Fourier series, then if the wave analyzer is tuned to the center frequency of one of the comb spikes comprising the signal spectrum, the servo loop locks the wave analyzer to this frequency. If the reference oscillator drifts, both the ultrasonic pulse rate frequency and the wave analyzer center frequency change in synchronism. The PLL corrects any drift within the wave analyzer's three local oscillators to an accuracy of ±10 Hz.

The timing and divider circuits are used to trigger both the ultrasonic pulser and the gates. The divider circuit consists of a divide by five and two divides by ten digital counters that reduce the reference oscillator frequency to 2 kHz. This 2-kHz signal is sent to the timing circuits where it simultaneously initiates a trigger pulse for the ultrasonic pulser and triggers the first of two adjustable monostable multivibrators arranged in series. The first multivibrator sets the gate delay, and then it triggers the second multivibrator which sets the gate width. The gate signal from the timing circuits is sent to a pair of double balanced mixers which perform the actual gating operation. When the gate is "on," the mixers pass the ultrasonic echoes with only slight attenuation. When the gate is "off," the mixers attenuate the echoes (up to about 80 dB). In this manner, the gate passes only those ultrasonic echoes of interest. The amplifier is inserted between the two mixers in order to avoid overloading the first mixer on strong signals. The output from the second mixer is supplied to the wave analyzer and to the CRT, where it is monitored.

The wave analyzer has three local oscillators and a square law detector that provide an output voltage proportional to the power at its center frequency. A local oscillator and mixer operating from 30 to 48 MHz tune the instrument from 10 kHz to 18 MHz. The constant difference frequency of 30 MHz

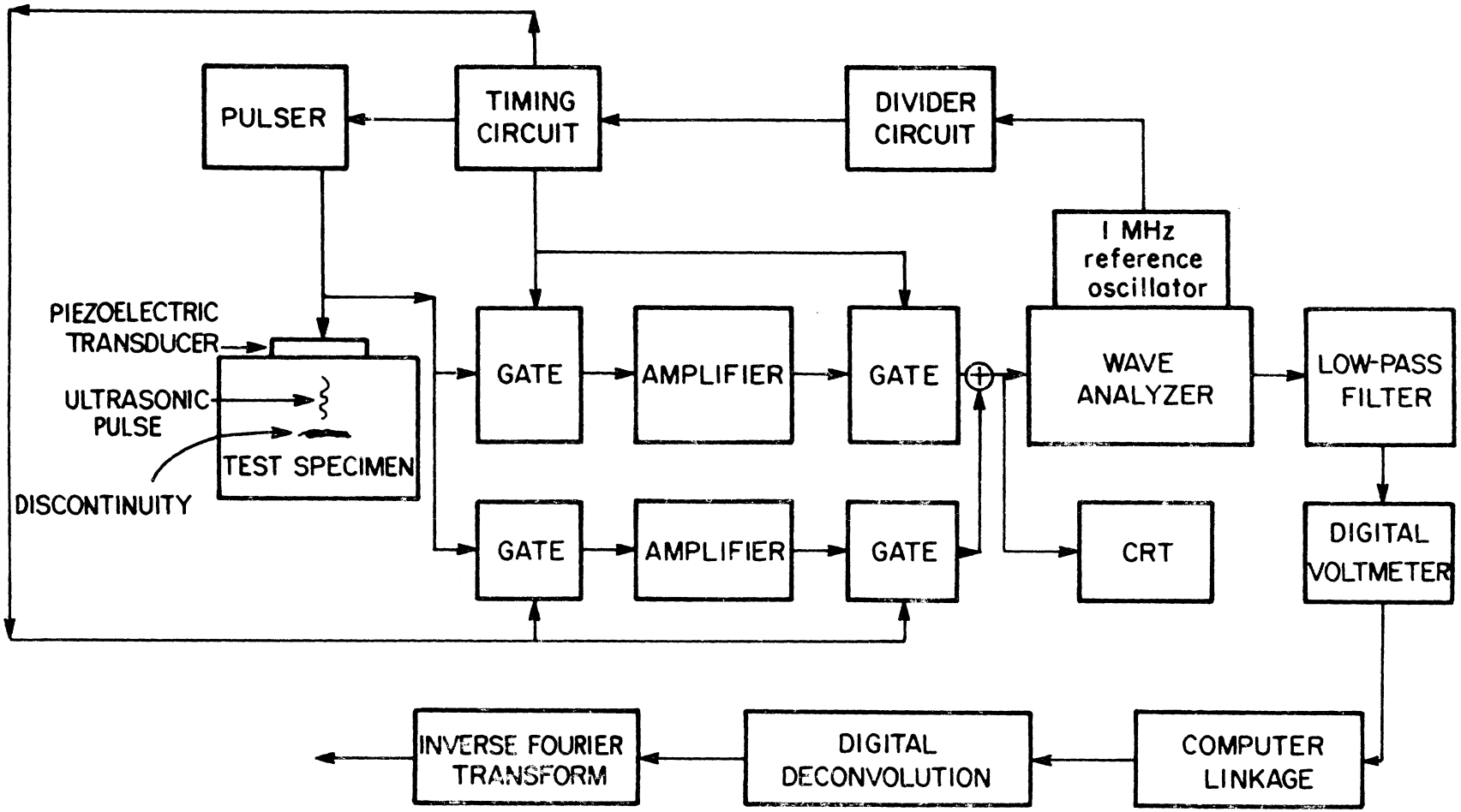

Figure 6. Schematic diagram of the complete ultrasonic and data processing systems.

is then mixed with another 30-MHz local oscillator. The difference frequency is filtered by a low-pass filter (typically 200-Hz bandwidth), mixed with a 250-kHz local oscillator, and applied to a square law detector. The output from the square law detector is proportional to the power in a 200-Hz bandwidth centered on the chosen frequency. The frequency tuning is indicated by a seven-digit counter.

The wave analyzer detector contains a 10-kHz bandwidth, low-pass filter. This filter has too much bandwidth to adequately limit the amplifier noise in the analyzer, so the detector output is additionally filtered by a 1-Hz bandwidth, third order Butterworth realization of an active, low-pass filter. An integrating digital voltmeter (DVM) capable of 10-bit resolution, digitizes the output from the 1-Hz filter and this digital data is entered directly into a storage file on a large, central computer using a remote terminal with an acoustic coupler.

The accuracy specification for the DVM was chosen by taking readings at four test frequencies over a period of about four hours. It was found that for 8-bit accuracy. the drift was about ±1/2 least significant bit. Also, as Gold and Rader (1969, page 101) show, the quantization noise variance for 8-bit accuracy is about 60 dB below the peak signal. This SNR is about equal to the SNR from the transducer thermal noise in a minimal noise situation. Thus, 8-bit accuracy is necessary to maintain the assumption that transducer thermal noise is the primary noise source.

For all the data that are reported here, the reference function is provided by the back surface reflection. A duplicate gating and amplifier system adjusts the reference function amplitude independently of the target amplitude. Two more monostable multivibrators together with another pair of double balanced mixers gate the back surface reflection to the summing junction. The amplifier gain is adjusted to make the reference function amplitude slightly greater than the maximum target echo amplitude. The target signal and the reference signal are additively combined and sent to the wave analyzer and to the CRT monitor.

A FORTRAN computer program controls the data conversion, deconvolution, and inverse Fourier transform procedures. Since the wave analyzer measures the power in discrete 10-dB bands, the DVM data contains a scale factor that must be used to calculate the actual power. This conversion process could also compensate for any nonlinearities in the wave analyzer, but it was experimentally established that the effect of such nonlinearities was less than the quantization noise and no compensation was used. The linearity was measured by inserting a stable (in amplitude and frequency) 1-MHz sine wave through a precision attenuator box into the wave analyzer. The linearity was measured only at this one frequency.

After conversion, the data are deconvolved using point by point division. This result is multiplied by a Hamming window function and Fourier transformed back into the time domain using an FFT algorithm. The final results are available as a sequence of numbers relating the absolute value of the amplitude and time or as a Calcomp graph of absolute amplitude versus time. The graph omits the data near t = 0 where the cross product terms are located.

At the present time, the program is interactive, as information about initial, final, and incremental frequency must be supplied. An interactive program was chosen for its experimental flexibility, but an automatic system seems just as feasible.

TEST SAMPLES

Two basic test targets established the feasibility of this system. The target in Figure 7a consists of three steps, B, C, and D, milled into a 150-mm high aluminum block. The steps are 3.18 mm wide and separated by 0.508 mm and 0.787 mm, respectively. These steps are intended to simulate closely spaced stringer inclusions. Step A or the back surface provide a reference function, depending on the transducer location. The target in Figure 7b consists of three, 1.6 mm, side-drilled holes, E, F, and G, randomly arranged in a 63.5-mm high aluminum block. The back surface provides the reference function. This target system is intended to simulate porosity. Both test targets are in the far field of all the transducers used in the following experiments.

An additional test target (not shown) is used to establish the expected SNR improvement. It consists of a 13-mm diameter, flat-bottom hole drilled into a plastic block loaded with metallic particles. The metallic particles scatter considerable energy out of the main beam, and, as a result, the echo from the flat-bottom hole is extremely weak and submerged in the transducer thermal noise.

The defect distance is defined as one half the acoustical path from the transducer to the reference target and back again minus one half the acoustical path from the transducer to the defect target and back again. Thus, defect distance equals the distance between the defect target and the reference target slightly modified by an obliquity factor. Defect distance is measured using both an ultrasonic and geometrical technique. The formula $d = 1/2\ cT$ is used to calculate the ultrasonic defect distance, where **c** is the ultrasonic velocity of propagation and T is the time of flight to the reference target minus the time of flight to the defect target. The geometrical defect distance is calculated using data provided by micrometer measurements of target position. For the three-step target in Figure 7a, a depth micrometer is used to measure the distance from each step to the back surface, and a standard micrometer is used to measure the total height of the block. For the three-hole target in Figure 7b, an optical microscope equipped with a micrometer translation stage is used to measure target position.

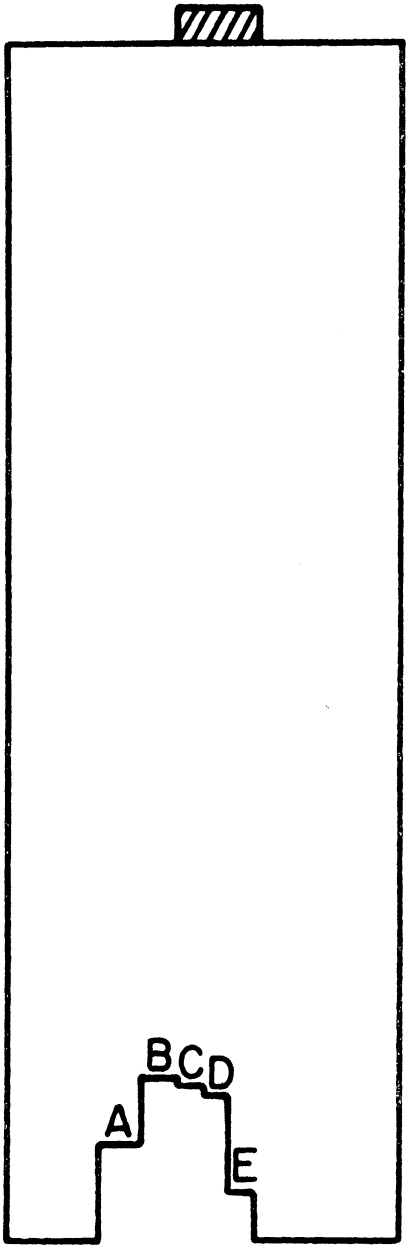

Figure 7a. Targets B, C, and D consist of a 0.508-mm and a 0.787-mm step in aluminum. Steps A and E supply a reference function.

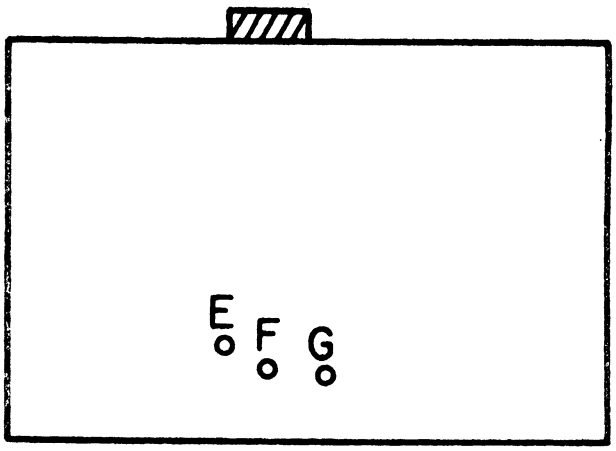

Figure 7b. Targets E, F, and G consist of three 1.6-mm diameter holes drilled in aluminum. Back surface supplies the reference function.

For the three-step target in Figure 7a, four different transducer positions are used. In the first position, denoted as position 1, the transducer center line is coincident with the left side of step B. In the second position, denoted as position 2, the transducer center line is coincident with the right side of step B. In the third position, denoted as position 3, the transducer center line is coincident with the right side of step C. And in the fourth position, denoted as position 4, the transducer center line is coincident with the right side of step D.

Since all the targets are located in the far field of the transducer, they are all insonified with a plane wave, but not all the targets will reflect a plane wave. The type of reflection process occurring when the three steps are insonified can be seen by considering an infinite, smooth surface with a step at the origin. For a transducer located far to the left of the origin, the surface is insonified with a plane wave, and, since there are no irregularities within the beamwidth of the transducer, a plane wave is reflected back to the transducer. This situation remains the same as the transducer is scanned toward the origin until the step comes within the transducer's beamwidth. Then both the upper and lower surfaces reflect the incident pulse, but the pulse from the upper surface is not received due to the finite size of the transducer. At this point, the upper surface would not be detected were it not for the fact that the corner of the step reflects a spherical wave. This spherical wave is received by the transducer (with an amplitude diminished by the inverse distance law), and the presence of the upper surface is detected, but with a diminished amplitude relative to the lower surface. As the scan is continued to the right, the plane wave pulse reflected from the upper surface is finally received by the transducer and both surfaces are indicated by about the same amplitude.

This analysis is important in calculating the acoustic distance to each step of the three-step target. If both surfaces of a step are reflecting plane waves, then the acoustic distance is the perpendicular distance from the transducer to the surface, plus the perpendicular distance from the surface to the transducer. But if the upper surface of the step is detected by the spherical wave reflected from the corner, then the acoustic distance is the perpendicular distance from the transducer to the step plus the oblique distance from the step to the transducer. Thus, for position 1 for the three-step target, the transducer is located directly over step A (the reference function) and step B, and these steps reflect plane waves. The plane waves reflected by steps C and D miss the transducer and these steps are detected only by the spherical waves reflected by the corner of each step. Likewise, in position 2, steps B and C reflect plane waves and step D and Step A (the reference function) reflect spherical waves; in position 3, steps C and D reflect plane waves and step B and step E (the reference function) reflect spherical waves; and in position 4, step E (the reference function) and step D reflect plane waves, and steps B and C reflect spherical waves. As is shown later in Figure 13, a small amplitude spherical wave reflection can be seen

from step A with the transducer in position 4. These transducer locations are noted in Table I and in the captions for Figures 9-13, and they account for the slightly different distances assigned to the same target for different transducer locations.

Uncertainties in the location of the peak value of the target display introduce an error in the ultrasonic distance measurement of approximately ±0.05 mm. Uncertainties in the transducer location introduce an error in the geometrical distance measurement of approximately ±0.075 mm. The micrometers used to provide the data for the geometrical distance calculations are all calibrated on a regular basis, and their error is assumed to be less than ±12 μm. For this reason, micrometer error will be neglected.

The ultrasonic velocity was independently measured using the test block shown in Figure 7a. Since the test block is only 26.1 mm thick, multiple reflections of one pulse within the test piece continue for four or five round trips when the transducer is placed on the front face. If two of these multiple reflections are gated into a spectrum analyzer, a sine wave modulated spectrum results. If as many multiple reflections as possible are gated into the spectrum analyzer, the sine wave modulation is "sharpened" into a series of spikes in the same way that a Fabry-Perot etalon "sharpens" the frequency selectivity of an optical interferometer.

A spectrum analyzer recording of this process is shown in Figure 8. The upper trace is the "sharpened" spectrum, the lower trace is a calibrated frequency comb. The frequency difference, Δ, between adjacent spikes is related to the ultrasonic velocity, c, and the thickness, d, according to the following formula.

$$c = 2d\Delta$$

Δ was measured by averaging over 22 different spikes and d was measured using a micrometer. Δ, and thus c, is estimated to be accurate to within ±0.5%. The value of c derived from this formula and used in all subsequent calculations is 6.28×10^6 mm/second.

PROCEDURE

The system shown in Figure 6 is operated in the following manner.

1. Place the transducer over a single point target. Take the echo return and apply it to the wave analyzer. Tune the wave analyzer to each comb tooth in the echo spectrum, digitize the measured power, and store in a computer for subsequent use.

TABLE I

COMPARISON BETWEEN ULTRASONIC AND MICROMETER DISTANCE MEASUREMENTS

Figure	Position	Target	Ultrasonic Distance in mm	Geometrical Distance in mm
9	2	B	7.90	7.75
		C	7.06	6.96
		D	6.43	6.38
10	2	B	7.98	7.75
		C	7.21	6.96
		D	6.58	6.38
11	1	B	7.72	7.67
		C	6.99	6.81
		D	6.25	6.22
12	3	B	14.1	14.0
		D	12.7	12.8
13	4	B	13.7	13.8
		D	12.6	12.7
14	••	E	10.2	10.2
		F	8.59	8.59
		G	7.47	7.16
15	••	E	10.1	10.2
		F	8.59	8.59
		G	7.21	7.16
17	4	B	13.8	13.9
		C	13.2	13.2
		D	12.6	12.7

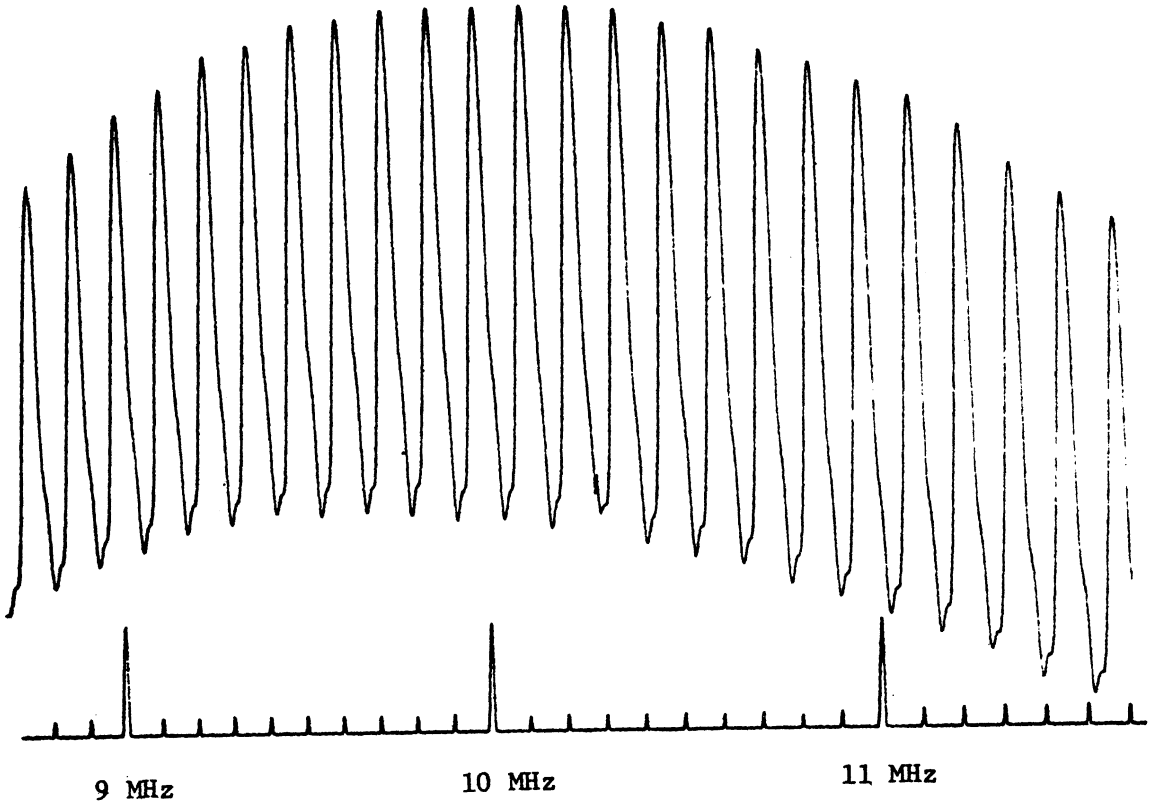

Figure 8. Power spectrum of the multiple reflections in a 26.1-mm thick aluminum block. Small pips on lower trace occur every 100 kHz.

2. Place the transducer over the unknown target. Using one gate system for the target echo and one gate system for the reference function, add these two signals and apply the combination to the wave analyzer. Tune the wave analyzer over the spectrum, digitize, and store the result in a computer as in step 1.

3. Point by point divide the digital power spectrum from step 2 by the digital power spectrum from step 1.

4. Multiply the result from step 3 by a Hamming window function and Fourier transform the signal back into the time domain. Now the signal can be displayed in any of the conventional ways (CRT, strip chart recorder, etc.).

Step 1 measures the function $S_1(f)$ in equation (8). If the medium has a negligible effect, $S_1(f)$ is the transducer power spectrum, sometimes called the transducer frequency response. Step 2 measures the function $S_2(f)$ in equation (12). Step 3 is the deconvolution procedure. In step 4, the Hamming window function weights the spectral data so as to provide minimal side-lobe level in the final time-domain display. Figure 12 shows an example where the side-lobe level is 32 dB below the peak signal, as compared with a predicted value of 42 dB.

IV. RESULTS

Figures 9-18 display the results obtained on the two test targets in Figure 7 and on the flat-bottom hole in the plastic block. Figures 9 through 13 use the three-step target in Figure 7a, Figures 14 and 15 use the three-hole target in Figure 7b, and Figure 18 uses the flat-bottom hole in the plastic block, Figures 16 and 17 are included primarily to illustrate points made in the theoretical development of the method. Four different transducers, two 10-MHz units, a 5-MHz unit, and a 2.25-MHz unit, were used in this experimental study. Their responses are shown in Figure 2. Both 10-MHz units are 6.4 mm in diameter. One unit, designated SFZ, is a zirconate-titanate ceramic unit with an impulse response shown in Figure 2b. The other unit, designated SCJ, is a special faced-ceramic unit with an impulse response pictured in Figure 2d. The exact construction of the SCJ unit is proprietary and hence no information about the unit is available. The 5-MHz unit is a 13-mm diameter, lead metaniobate crystal with an impulse response pictured in Figure 2c. The last transducer, a 13-mm diameter, 2.25-MHz zirconate-titanate ceramic unit designated SFZ, has the impulse response shown in Figure 2a. The particular transducer used in each instance is indicated in the figure caption.

With one exception, the format of Figures 9-18 is the same. The photographs in the figures show the CRT monitor (see Figure 6) taken during the data acquisition phase of the experiment. This waveform supplies the actual raw data used in the computer processed data graphed beneath it. The computer processed data are presented as a 65% reduction of a Calcomp graph of the final, processed output. This output is also available in tabular form (not included), and it is from this table that the distance data for each target indication is calculated. Each target indication on the Calcomp graph is identified with a step or hole as labeled in Figure 7. Since the reference function is preceded by the simulated defect, the time scale on the computer processed data is inverted. On the oscilloscope photographs, the targets appear in natural order—the simulated defect precedes the reference function. On the Calcomp graph, the reference function appears at $t = 0$ (it has been masked off in order to emphasize the simulated defect), and the simulated defect follows. Thus, when temporal relationships between the two graphs are being compared, either the Calcomp graph or the oscilloscope photograph must be reflected through the reference function. With a little more sophisticated manipulation of the Calcomp plotter, this problem could be avoided. The time scale of each graph is noted in the caption. The ordinate of the oscilloscope photograph is relative amplitude. Since the computer output is a complex-valued function, the Calcomp ordinate is the absolute value of the amplitude normalized to the largest target indication. Detailed information on each experiment is reported elsewhere (Seydel, 1972).

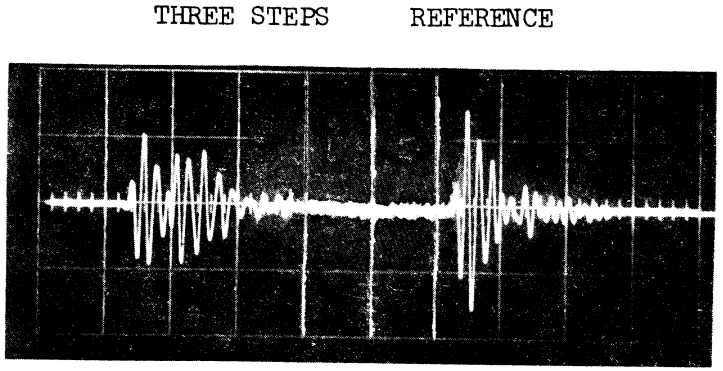

Figure 9a. RF "A" scan presentation of the three-step and reference echoes using the 10-MHz SFZ transducer in position 2. Time scale is 500 ns/div.

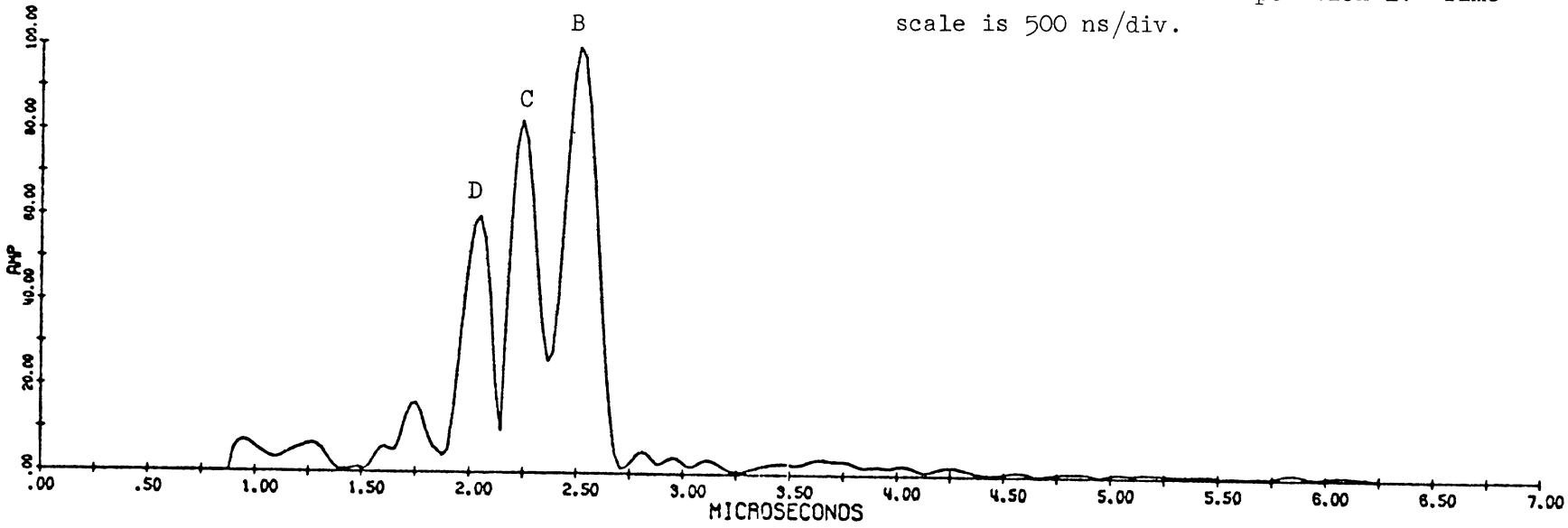

Figure 9b. Computer drawn graph of the three-step target obtained by processing the data shown in Figure 9a.

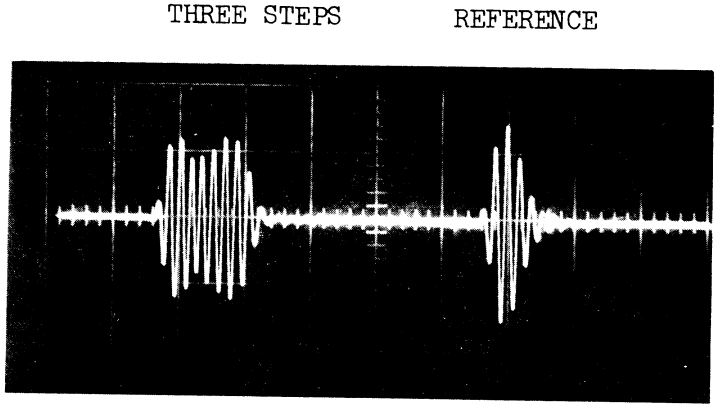

Figure 10a. RF "A" scan presentation of the three-step and reference echoes using the 10-MHz SCJ transducer in position 2. Time scale is 500 ns/div.

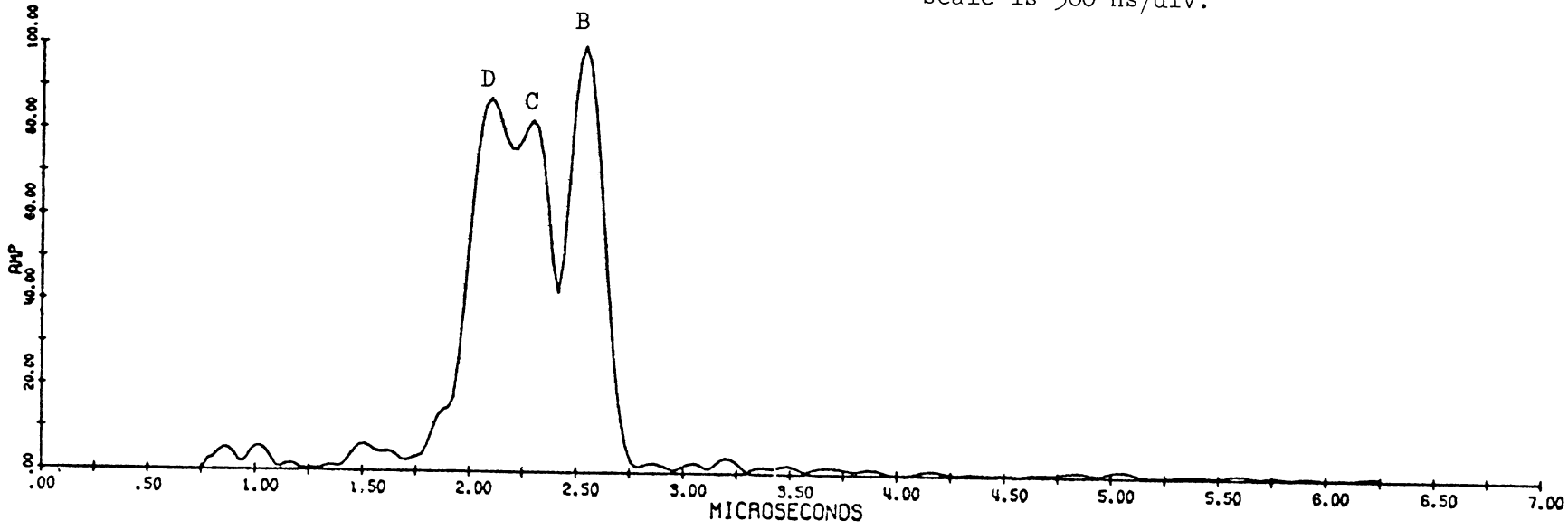

Figure 10b. Computer drawn graph of the three-step target obtained by processing the data shown in Figure 10a.

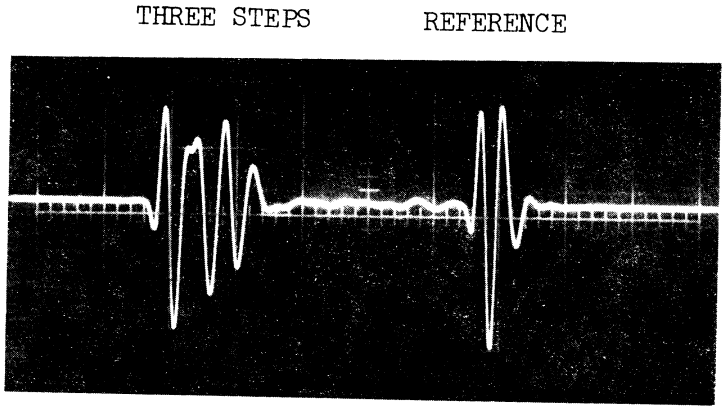

Figure 11a. RF "A" scan presentation of the three-step and reference echoes using the 5-MHz lead metaniobate transducer in position 1. Time scale is 500 ns/div.

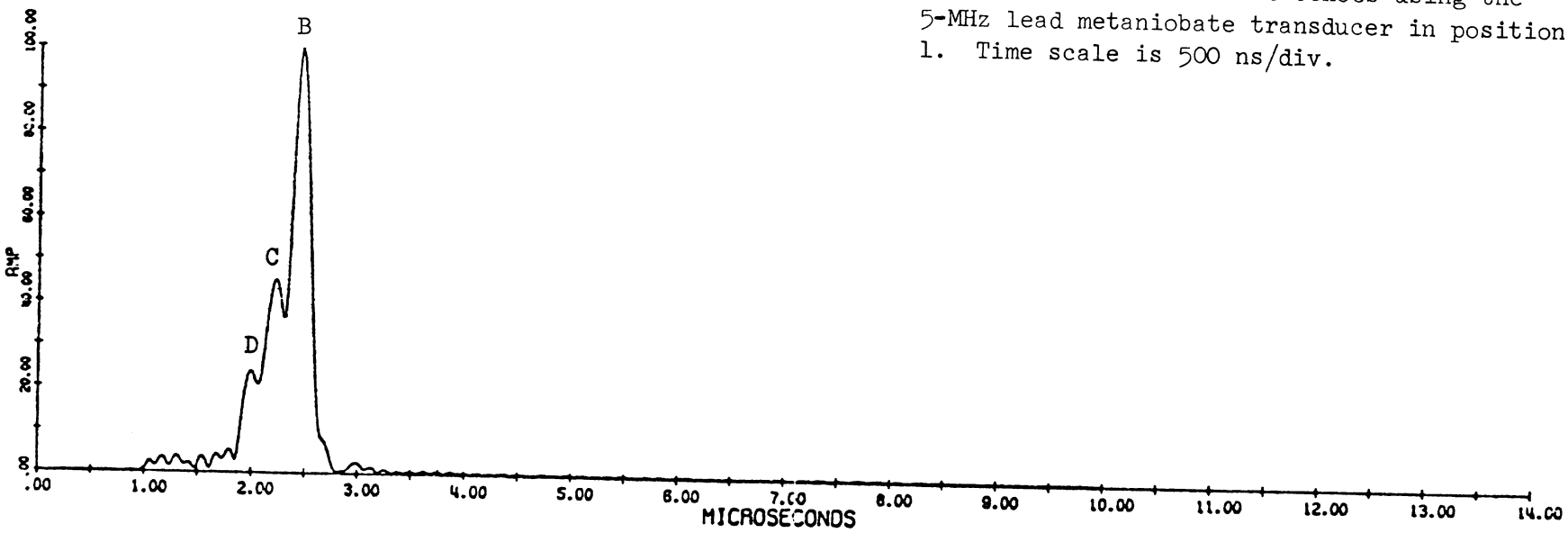

Figure 11b. Computer drawn graph of the three-step target obtained by processing the data shown in Figure 11a.

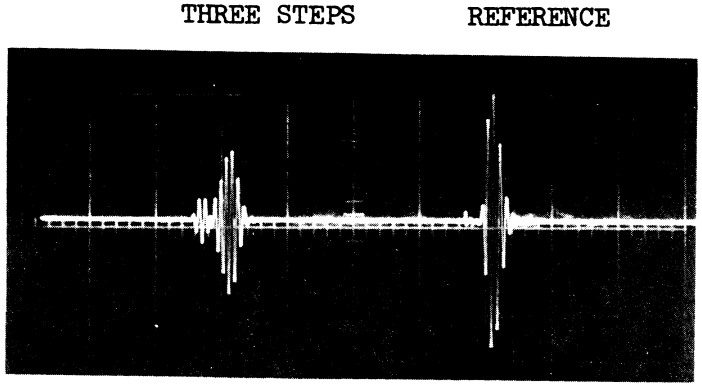

Figure 12a. RF "A" scan presentation of the three-step and reference echoes using the 10-MHz SCJ transducer in position 3. Time scale is 1.0 μsec/div.

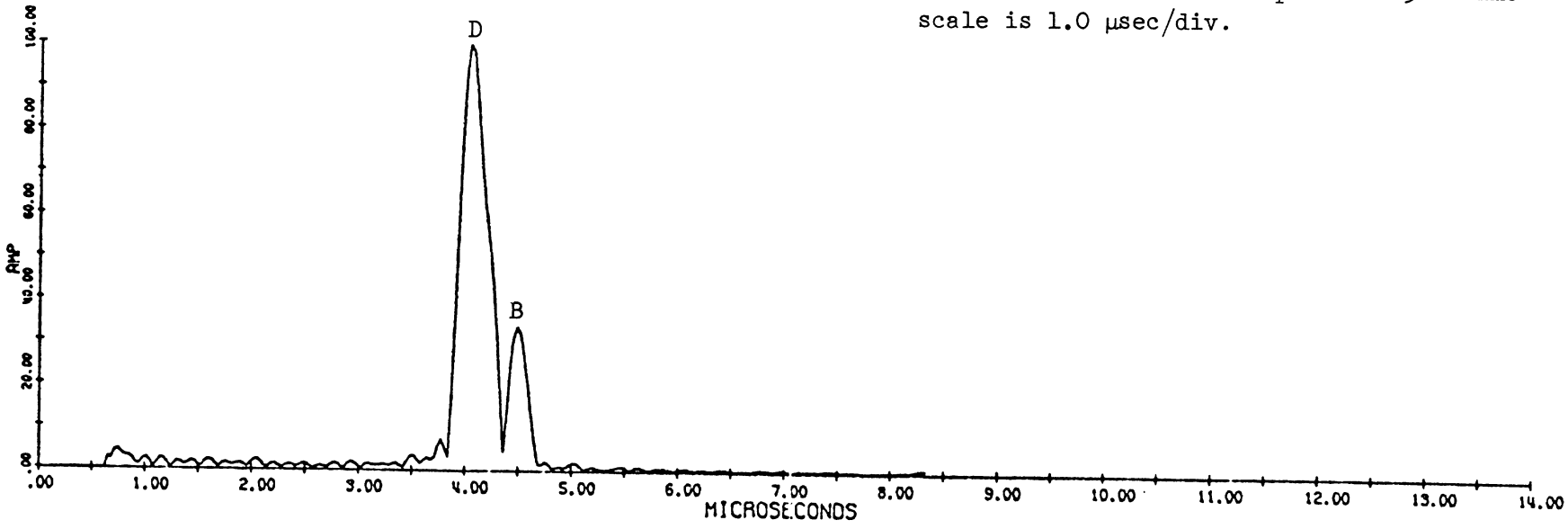

Figure 12b. Computer drawn graph of the three-step target obtained by processing the data shown in Figure 12a.

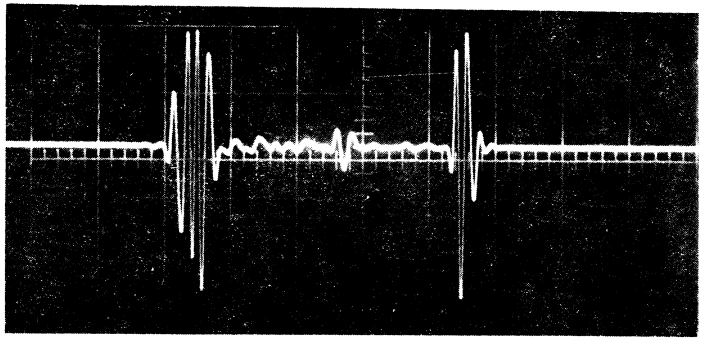

Figure 13a. RF "A" scan presentation of the three-step and reference echoes using a 5-MHz lead metaniobate transducer in position 4. Time scale is 1.0 μsec/div.

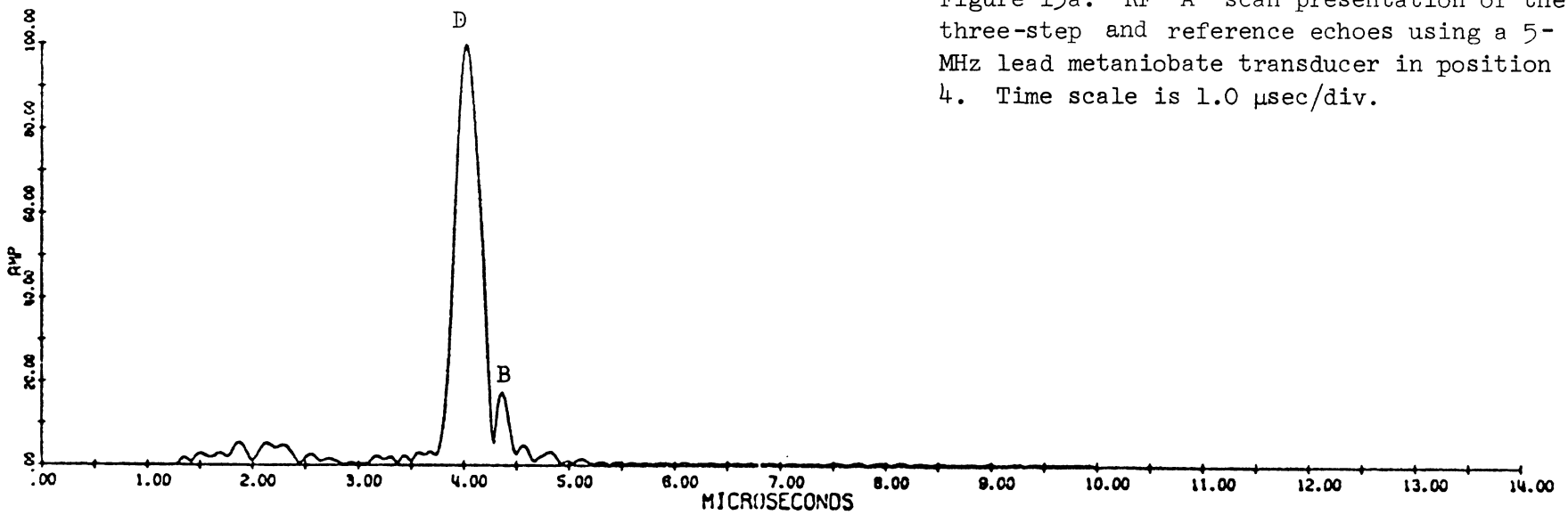

Figure 13b. Computer drawn graph of the three-step target obtained by processing the data shown in Figure 13a.

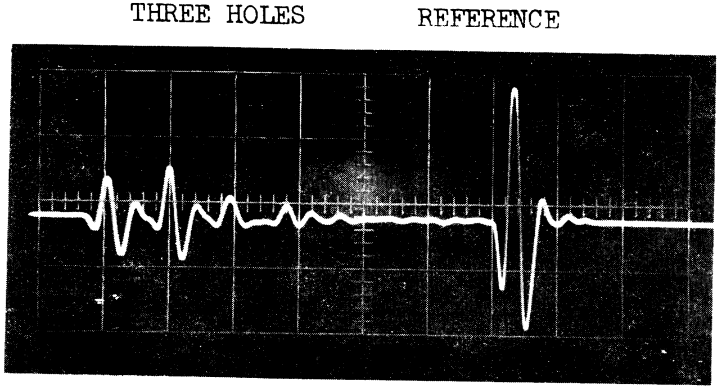

Figure 14a. RF "A" scan presentation of the three-hole and reference echoes using a 5-MHz lead metaniobate transducer. Time scale is 500 ns/div.

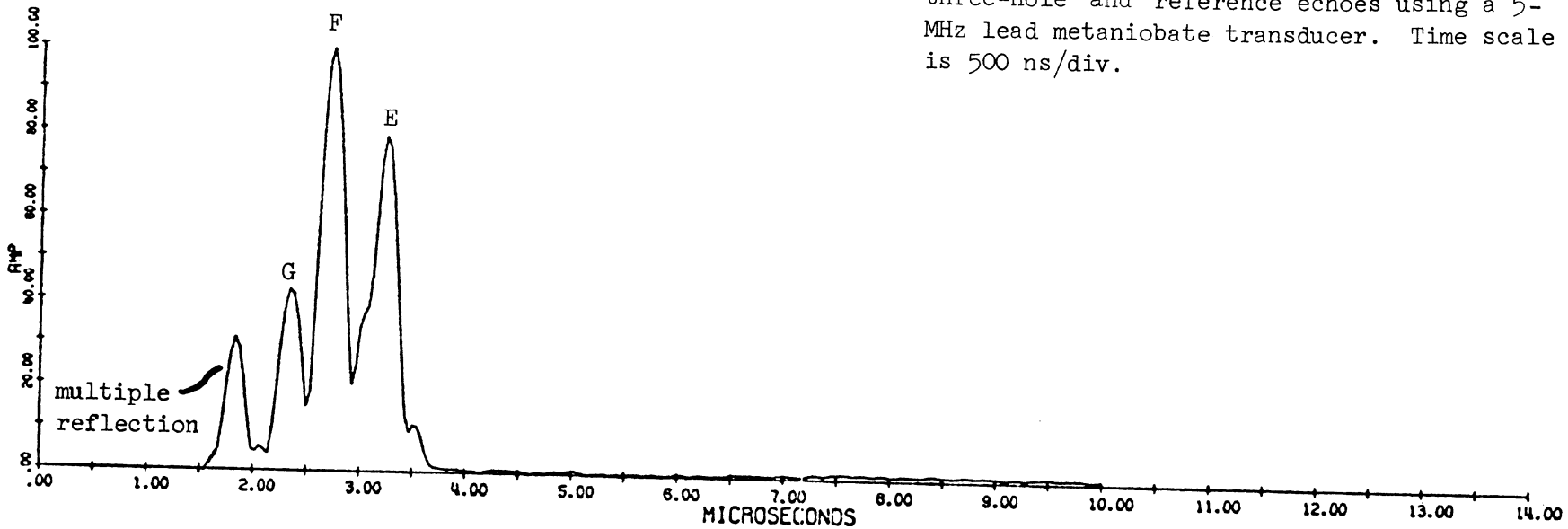

Figure 14b. Computer drawn graph of the three-step target obtained by processing the data shown in Figure 14a.

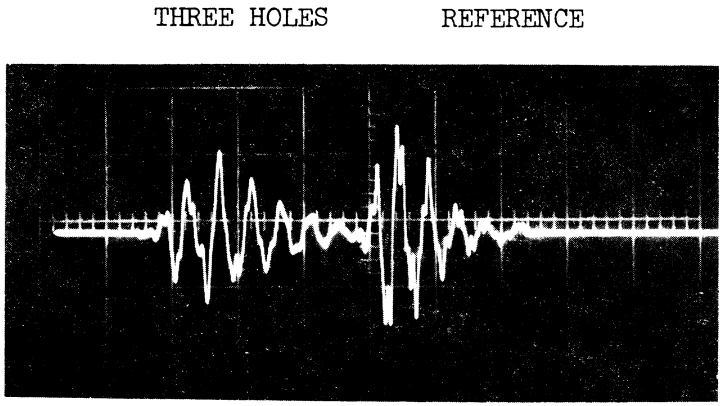

Figure 15a. RF "A" scan presentation of the three-hole and reference echoes using the 2.25-MHz SFZ transducer. Time scale is 1.0 μsec/div.

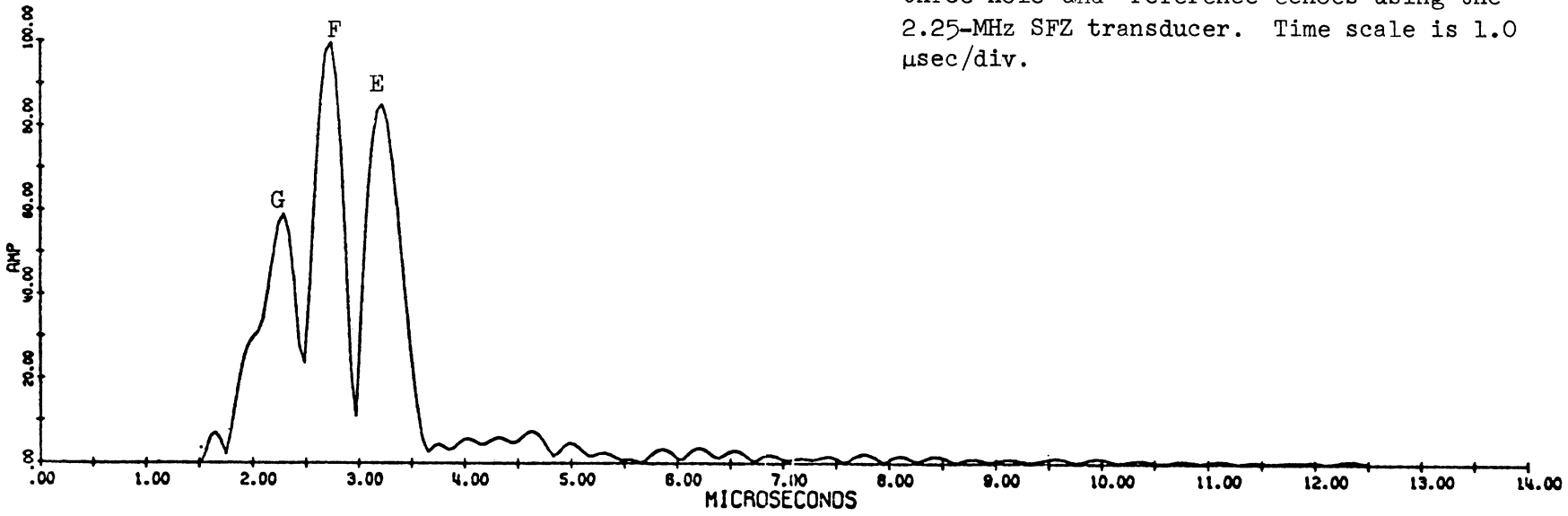

Figure 15b. Computer drawn graph of the three-step target obtained by processing the data shown in Figure 15a.

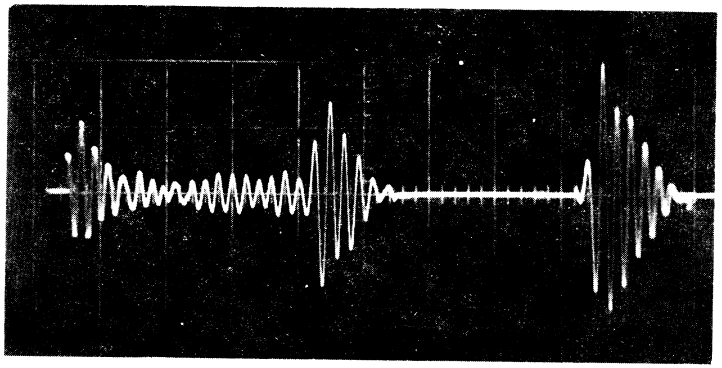

Figure 16a. RF "A" scan presentation of the target and reference echoes from a cast iron sample using the 2.25-MHz SFZ transducer. Time scale is 2.0 μsec/div.

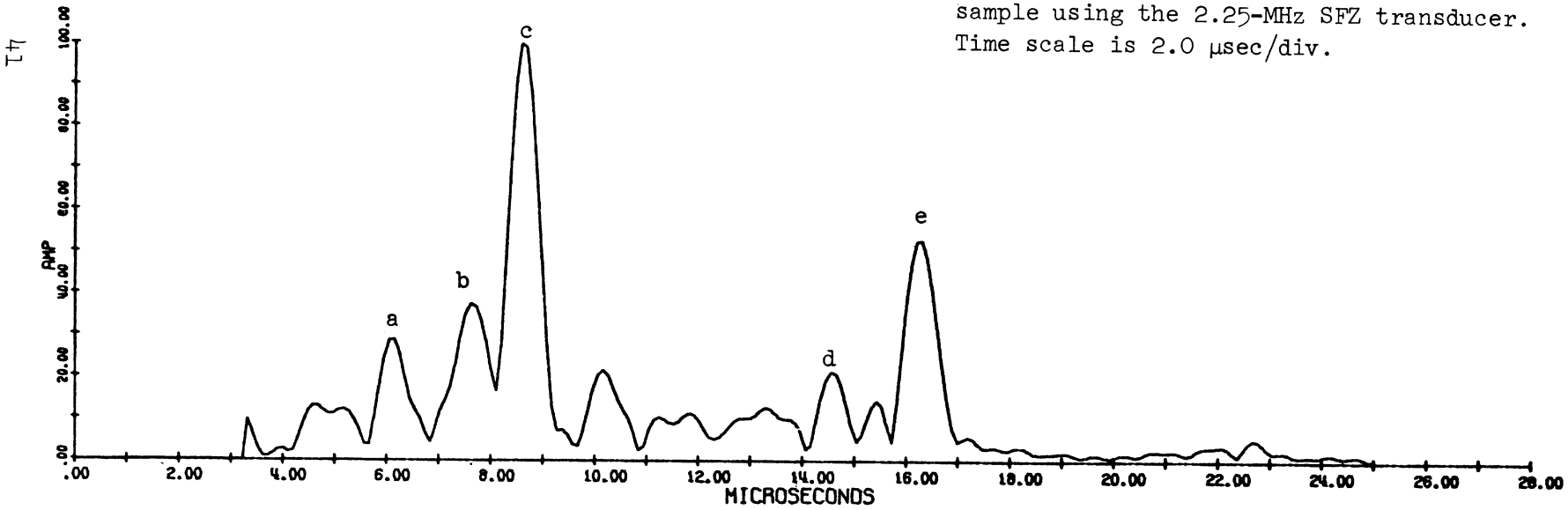

Figure 16b. Computer drawn graph of cast iron target obtained by processing the data shown in Figure 16a.

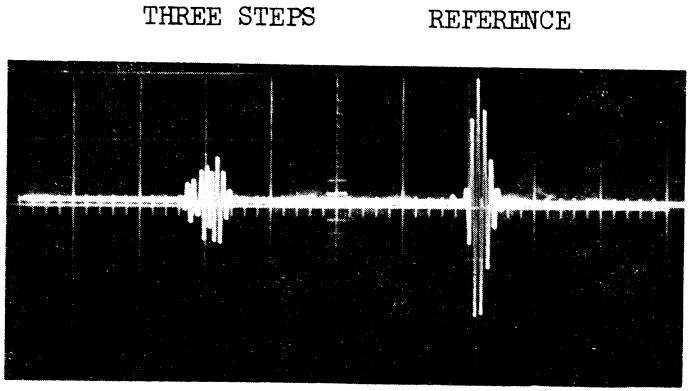

Figure 17a. RF "A" scan presentation of the three-step and reference echoes using the 10-MHz SCJ transducer. Time scale is 1.0 μsec/div.

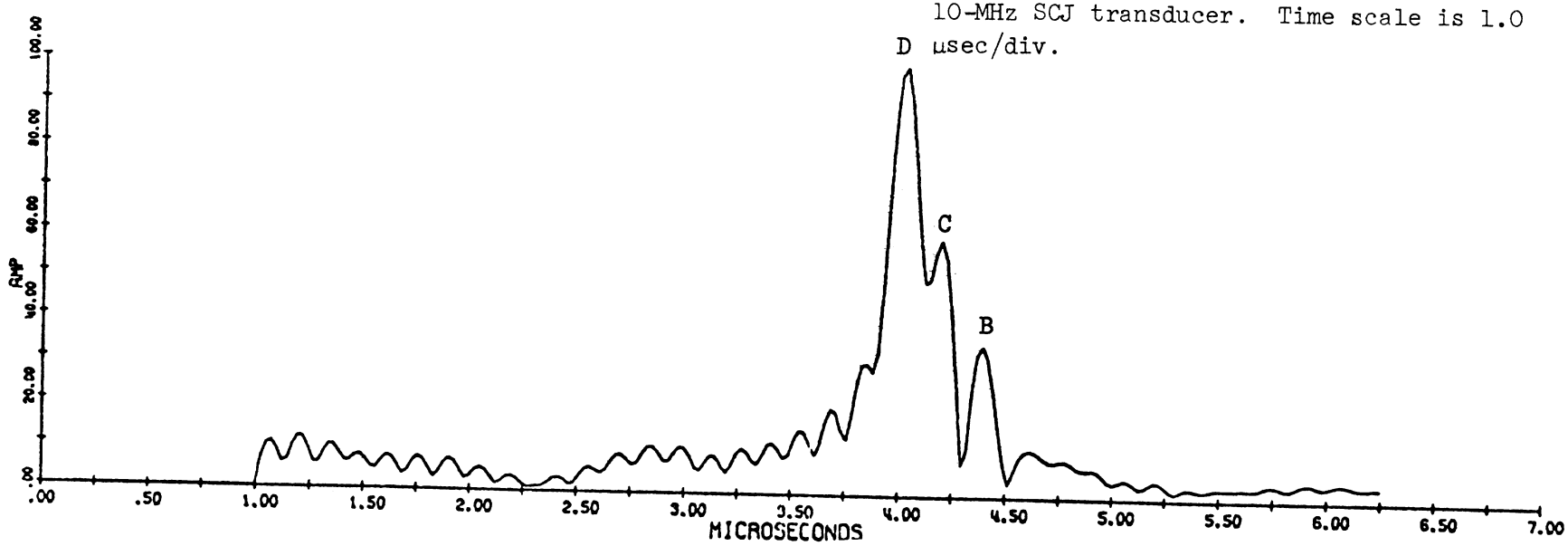

Figure 17b. Computer drawn graph of the three-step target obtained by processing the data shown in Figure 17a.

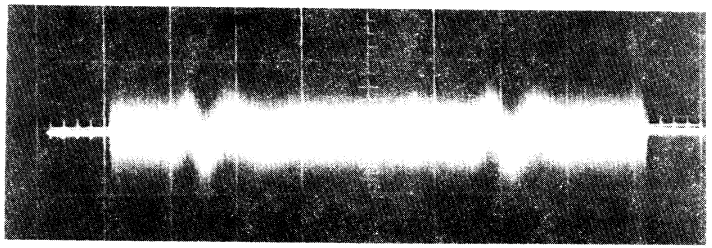

Figure 18a. RF "A" scan presentation of the target and reference echoes from the plastic block using a 5-MHz lead metaniobate transducer. Time scale is 2.0 μsec/div.

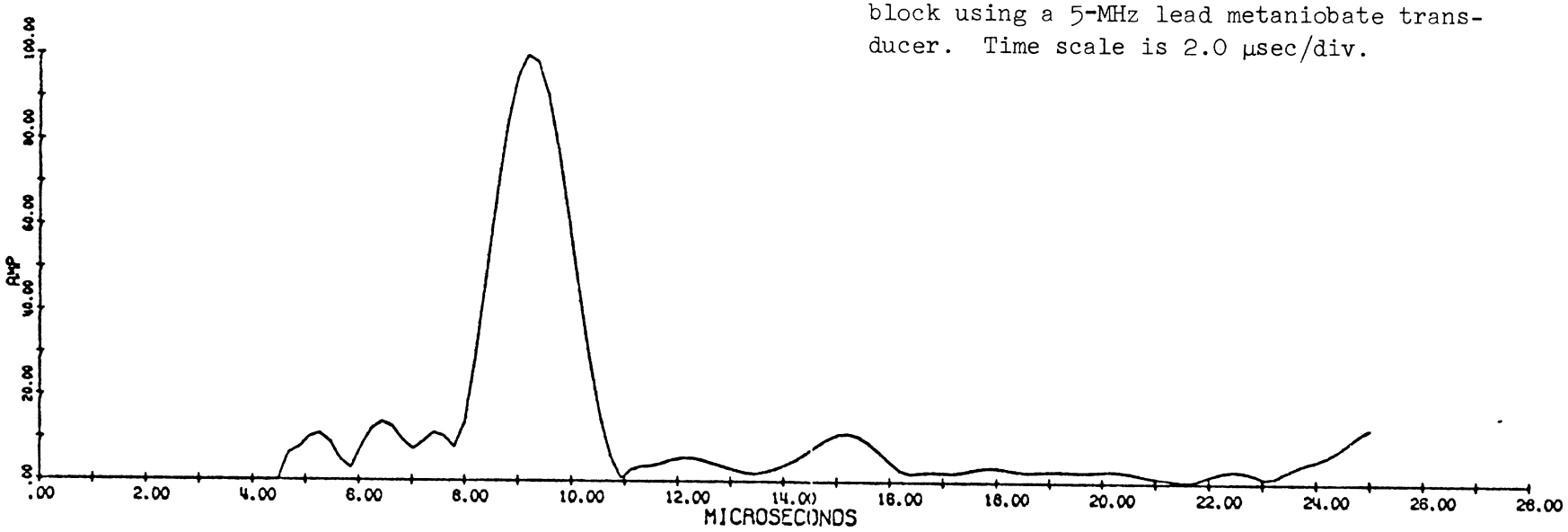

Figure 18b. Computer drawn graph of the milled step in the plastic block obtained from the data in Figure 18a.

V. DISCUSSION OF RESULTS

The computer processed data displayed in Figures 9-18 is superior to a conventional "A" scan display in four crucial areas, namely, the accurate measurement of target distance, transducer longitudinal resolution, transducer independence, and transducer SNR. These are considered in detail below.

DISTANCE MEASUREMENT

Table I (p. 30) displayed the ability of the data processing system to provide accurate measurements of the distance to a defect. As discussed in Section III, the ultrasonic distance measurement has an error bound of ±0.05 mm, and the geometrical distance measurement has an error bound of ±0.08 mm. An uncertainty of ±0.5% in the ultrasonic velocity also contributes to the error in the ultrasonic distance. Since the velocity error is the same for all common paths, this error applies only to the distance between the reference and defect targets. For defect targets whose distance is about 7.0 mm the ultrasonic velocity error bound is ±0.08 mm. Thus, the error bound of the ultrasonic distance is ±0.13 mm, and the error bound of the geometrical distance is ±0.08 mm. Of the twenty-two entries in Table I, nineteen of them are within the combined error bound of ±0.21 mm. If the error bound is lowered to ±0.15 mm, seventeen of the twenty-two entries are included, and if the error bound is lowered to ±0.10 mm, sixteen of the twenty-two entries are included. A majority of the excluded entries comes from Figure 10. For this example, the average relative error is only 0.025 mm while the average absolute error is 0.23 mm. It could be contended that this large absolute error is due to a thick wear plate on this particular transducer, since the wear plate thickness is measured by the ultrasonic system but not by the micrometer, but the same transducer is used in Figures 12 and 17, and neither of these samples shows the same effect.

In a conventional ultrasonic system, comparable measurements could be made by choosing a particular timing point (such as an axis crossing) on the waveform of the returning echo. In a medium with little frequency dependent attenuation, the waveform will retain the same shape, and such a system can equal or exceed the accuracy achieved by the data presented here. But when comparing the two systems, three points must be kept in mind. First, for comparison purposes, the appropriate error bound on the processed ultrasonic data is ±0.05 mm since both systems are subject to the same error in ultrasonic velocity. Second, because of the error bounds on the other quantities, no attempt was made to increase the accuracy of the processed data by using numerical interpolation. And third, any frequency-dependent attenuation in the medium causes a distance-dependent error in the conventional system. Serabian (1968) discusses this problem and presents some experimental data to

verify the effect. But due to the media compensating qualities of the processing system, the processed data has an error which is a function only of the relative distance between the reference and defect targets and not of the absolute distance to the defect target.

RESOLUTION

As shown in Section II, the transducer longitudinal resolution can be improved by as much as a factor of ten using a deconvolution procedure. The best examples of such an improvement in resolving power are Figures 9, 11, and 15. In Figure 9a, the back surface reflection shows that the transducer rings for about 0.6 μsec. This time duration implies a distance resolution of about 2.0 mm, a reasonable figure since the conventional "A" scan display in Figure 9a does not resolve the three-step targets with a separation of 1.37 mm. The computer processed display in Figure 9b completely resolves all three steps, and, thus, it demonstrates a resolution greater than 0.58 mm (from Table I). Using the fact that the maximum resolution equals the velocity of propagation divided by twice the bandwidth (c/2BW), the computer processed data in Figure 9b has a maximum resolution of 0.36 mm. In this example, the deconvolution process increases the resolution by a factor of six. In Figure 11a, the back surface reflection shows a resolution of about 0.6 μsec or about 2.0 mm. The computer processed data barely resolves all three steps, and it thus demonstrates a resolution greater than 0.58 mm. In fact, the resolution is probably more nearly 0.50 mm since the 0.58-mm step has about one quarter the amplitude of the largest echo and resolution is usually defined for equal strength targets. Using this assumption, the deconvolution process increases the resolution by a factor of four. In Figure 15a, the back surface reflection shows a resolution of about 1.5 μsec or about 5.1 mm. The computer processed data completely resolves all three holes, and it thus demonstrates a resolution greater than 1.4 mm. Again, if the expression c/2BW is used to establish the greatest possible resolution, the computer processed data in Figure 15b has a maximum resolution of about 1.0 mm. In this example, the deconvolution process increases the resolution by a factor of five.

Figures 10, 12, 13, and 14 also demonstrate corresponding increases in resolution. In Figures 12 and 13, all three steps are not resolved even though, as the data in Table II show, the maximum resolution is adequate. It is believed that for these two cases, the transducer was placed in such a position that the echo returned from one or two of the steps was extremely weak in relation to the primary echo.

TABLE II

MAXIMUM RESOLUTION EXPECTED FOR THE COMPUTER PROCESSED DATA IN FIGURES 9-15

Figure	c/2BW in mm
9	0.36
10	0.41
11	0.48
12	0.38
13	0.41
14	0.99
15	0.97

Thus, the computer processed data have about five times the resolution of the corresponding unprocessed data. This falls short of the factor of ten improvement expected from the deconvolution procedure because the power spectral response of the transducers used in this experiment decreases more rapidly than the Lorentzian response postulated in the theoretical analysis. The resolution could be further increased by extending the bandwidth over which the deconvolution procedure is applied. For the experimental data presented here, the bandwidth was determined by the maximum and minimum power levels accepted by the wave analyzer. The upper power level was determined by the necessity of limiting the intermodulation products, and the lower power level was determined by the instrument sensitivity. For a particular transducer, these two power levels determined the upper and lower frequency cutoffs and hence the deconvolution bandwidth. If the deconvolution products could be decreased or the sensitivity increased, the resolution could be correspondingly increased.

The above conclusions concerning resolution improvement are drawn by comparing the RF "A" scan display with the computer processed data. If the comparison is made between the processed data and a rectified, filtered display, the resolution improvement is even more dramatic. Figure 19 shows a rectified, filtered display of the three-hole target using the same 5 MHz transducer used in Figure 14. The transducer is located directly above the center hole, exactly as in Figure 14. While the rectified display shows the possibility of two different targets, it does not meet the industry specifications for resolution. Thus, the rectified video display does not resolve two targets 3.1 mm apart while the processed display has a maximum resolution of 0.48 mm (From Table II, Figure 14). This represents an improvement factor of at least six, and, quite possibly, even as much as eight or ten.

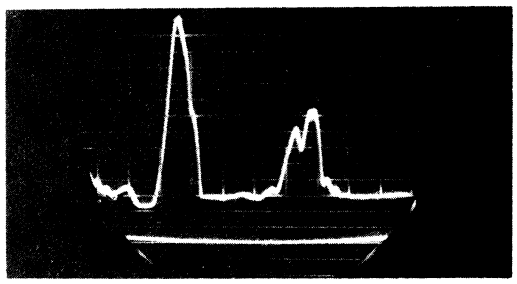

Figure 19. Rectified video display of the three-hole target in Figure 7b using the 5-MHz transducer in Figure 2c.

TRANSDUCER-INDEPENDENT DISPLAY

The ability of the data processing system to provide an output display that is almost independent of the ultrasonic transducer is seen by comparing Figures 14 and 15 and Figures 10 and 11. First, compare the target echo in Figure 14a with the target echo in Figure 15a. The echoes are dramatically different mainly because the two echoes come from a 5-MHz and a 2.25-MHz transducer, respectively. Also, the 5-MHz transducer almost resolves the three holes while the 2.25-MHz transducer does not. Next, compare the computer processed data in Figure 14b with the computer processed data in Figure 15b. Except for the strong multiple reflection in Figure 14b, the two displays are qualitatively identical. There are some quantitative differences in echo strength and position probably due to minor differences in transducer location, but the form of the display is the same for two transducers of different operating frequency. The same comparison process can be used for Figure 10, a 10-MHz transducer, and Figure 11, a 5-MHz transducer, although in this case, the quantitative differences are more substantial.

To a greater or lesser extent, all the computer processed data in Figures 9b-15b illustrate the same transducer independent display. In every case, a single target is represented by a single blip. The ringing response of the transducer is almost completely removed since, in one example, the experimentally measured side-lobe level is 32 dB below the primary response. Also, this improved display technique is accompained with a simultaneous increase in resolution. This distinguishes the present data processing technique from the conventional rectified video display where display uniformity is achieved only with a loss of resolution.

SNR IMPROVEMENT

Figure 18 demonstrates the capability of the data processing system to increase the SNR. Figure 18a is an "A" scan presentation of the echo from

a flat-bottom hole located in a plastic block loaded with metallic particles. The metallic particles, having a much greater acoustic impedance than the plastic, cause considerable scattering. This scattering decreases the echo amplitude to the point where it is comparable to the thermal noise generated in the transducer and associated electronics. This condition is shown in Figure 18a. Figure 18b shows the computer processed data. The data processing used in this example is exactly the same as that used in all the previous examples. The unprocessed signal is estimated to have a SNR of one. The SNR for the processed data is difficult to estimate since certain sections of the graph appear to be attributable to spurious signals. For instance, the blip at 15 μsec is almost certainly due to a slight imbalance in the balanced mixer which allows the gate signal to transfer to the output, while the signal between 4 and 8 μsec could be due to small imperfections on the flat-bottom hole. If these ambiguities are included in the calculation of the noise power, the SNR (peak signal to RMS noise) is 20 dB. If the ambiguities are excluded, the SNR is 28 dB. The latter figure is probably more representative of the system capability. Thus, the data processing system has improved the SNR by 28 dB, as compared with a predicted improvement of 37 dB. A close examination of the unprocessed data in Figure 18a reveals a pulse duration of about 3.2 μsec. The corresponding time resolution in the processed display is about 1.6 μsec. Thus, the computer processed display shows a factor of two improvement in resolution achieved simultaneously with a 28-dB improvement in SNR.

The processed data in Figures 12 and 13 also demonstrated good SNR. In Figure 12, the signal between the targets and the back surface reflection has been gated out. Thus, the graph of the processed data from 1.0 to 3.5 μsec gives a good indication of the amount of noise introduced by the deconvolution process alone. The SNR (peak signal to RMS noise) in this area is 37 dB. In Figure 13, the signal between the targets and the back surface reflection is allowed to pass. The echo indications near 2.0 μsec can be identified with step A in Figure 7a. In both figures, the SNR in the area following the targets is excellent (about 45 dB).

COMPENSATION FOR A SCATTERING MEDIUM

The effect of a scattering medium upon the test results was briefly considered in Section II. Equation (13) was derived to show the quantitative effect of scattering on the data collected from the wave analyzer. Carrying the derivation a few more steps shows that

$$S(f) = M_2(f)M_2^{+}(f)G(f)G^{+}(f) + 1 + e^{-i2\pi fT}$$

$$M_2^{+}(f)G^{+}(f) + e^{i2\pi fT}M_2(f)G(f) \qquad (27)$$

where S(f) is defined as before and

$$M_2(f) = \frac{M_1^2(f)}{M^2(f)} \tag{28}$$

Equation (27) demonstrates the effect of a scattering medium on the output from the complete data processing system. This effect will be illustrated by expressing equation (28) in terms of the material properties of the aluminum test sample and inserting this result into equation (27) under the condition that a single point discontinuity is insonified.

$M_2(f)$ can be expressed as a function of the material properties of aluminum by using the equation relating attenuation and frequency shown below (Mason, 1950, page 414).

$$\alpha(f) = B_1 f + B_2 f^4 \tag{29}$$

B_1 and B_2 are functions of the material structure. Since $\alpha(f)$ is the attenuation coefficient expressed in dB/mm, then

$$\alpha(f) = [d \log M(f)]^{-1} \tag{30}$$

where d is the distance of travel and M(f) is the usual amplitude transmission function for a scattering medium as shown in Figure 1. Rearranging equation (30) gives

$$M(f) = e^{-d\alpha(f)} \tag{31}$$

and if equation (31) is substituted into equation (28), then

$$M_2(f) = e^{-2(d_1-d)\alpha(f)} \tag{32}$$

where $d_1 - d$ is the distance from the discontinuity to the reference function.

In spite of the particular form of $\alpha(f)$, this model of the scattering process demonstrates that the data processing system compensates for any scattering which occurs over an acoustic path common to both the discontinuity

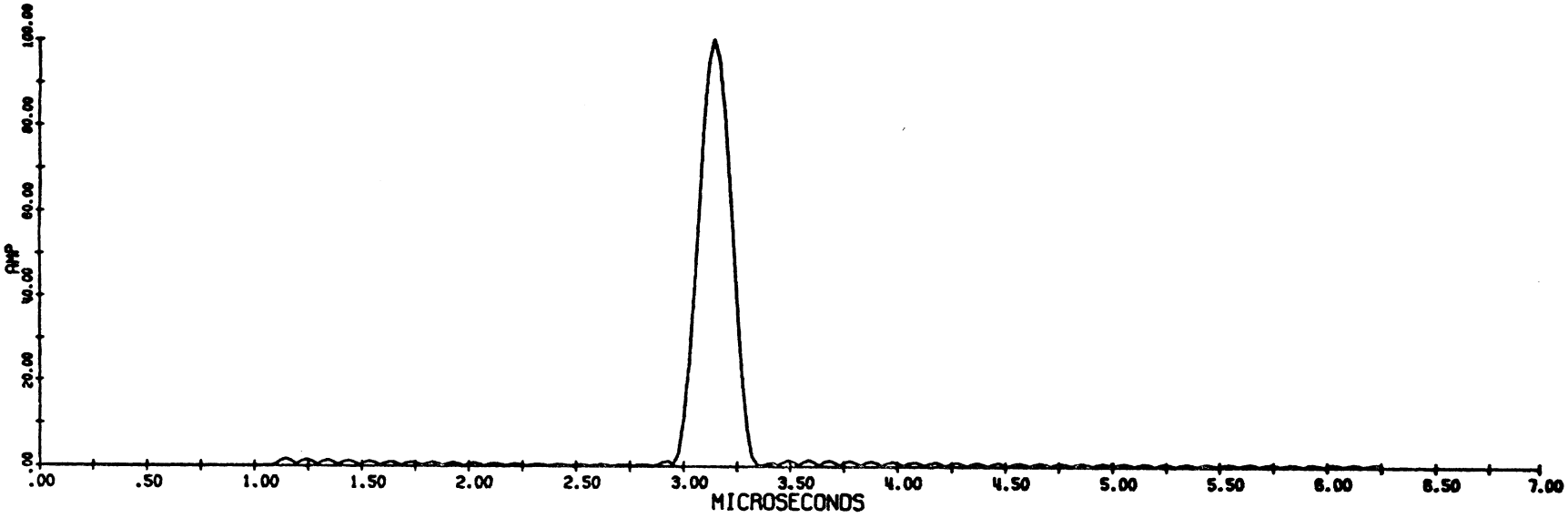

Figure 20. Computer simulation of the effect of scattering on a single target with $d_1 - d = 0.0$ mm.

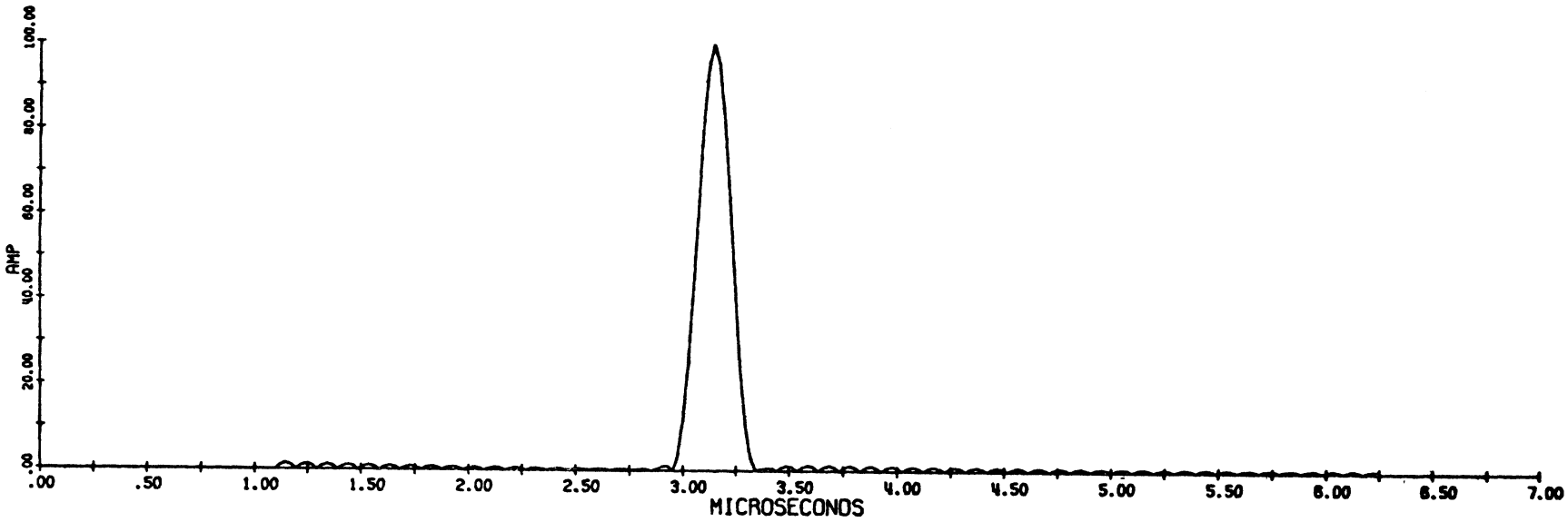

Figure 21. Computer simulation of the effect of scattering on a single target with $d_1 - d = -12.7$ mm.

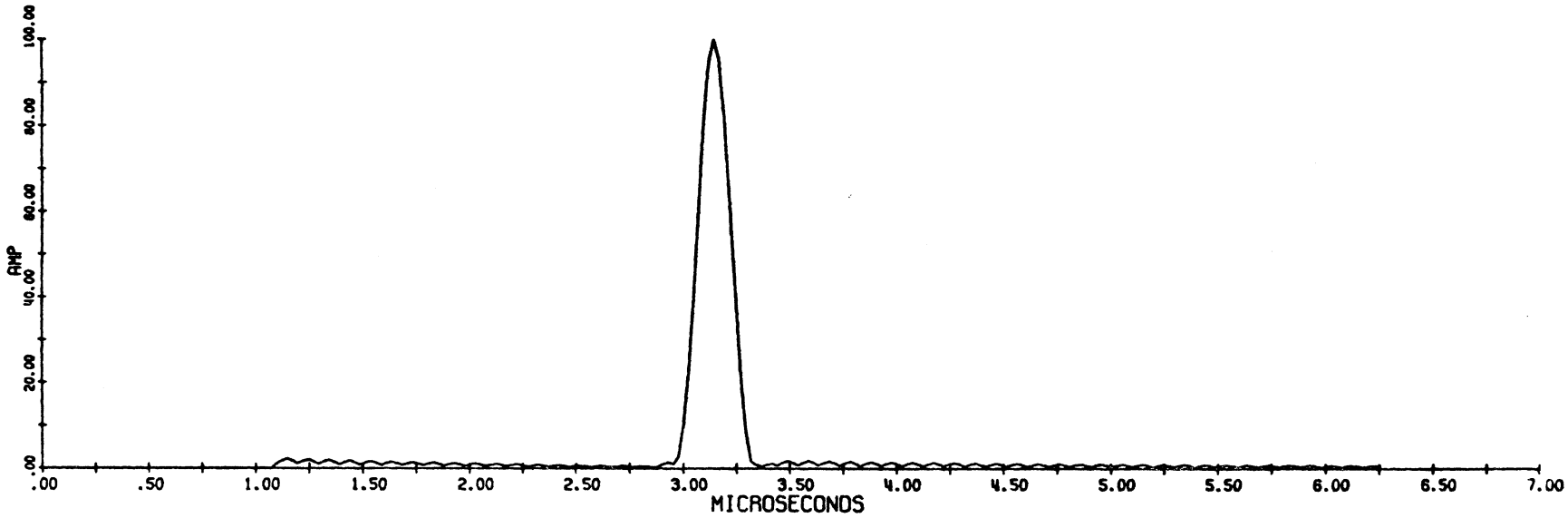

Figure 22. Computer simulation of the effect of scattering on a single target with $d_1 - d = -25.4$ mm.

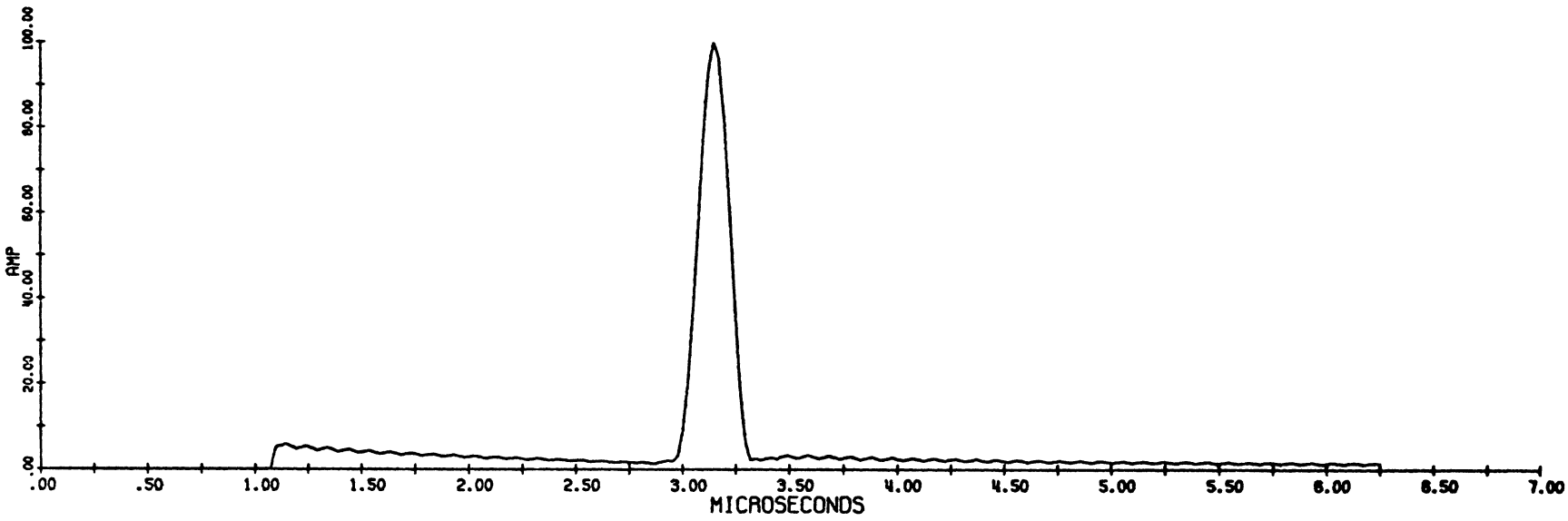

Figure 23. Computer simulation of the effect of scattering on a single target with $d_1 - d = -50.8$ mm.

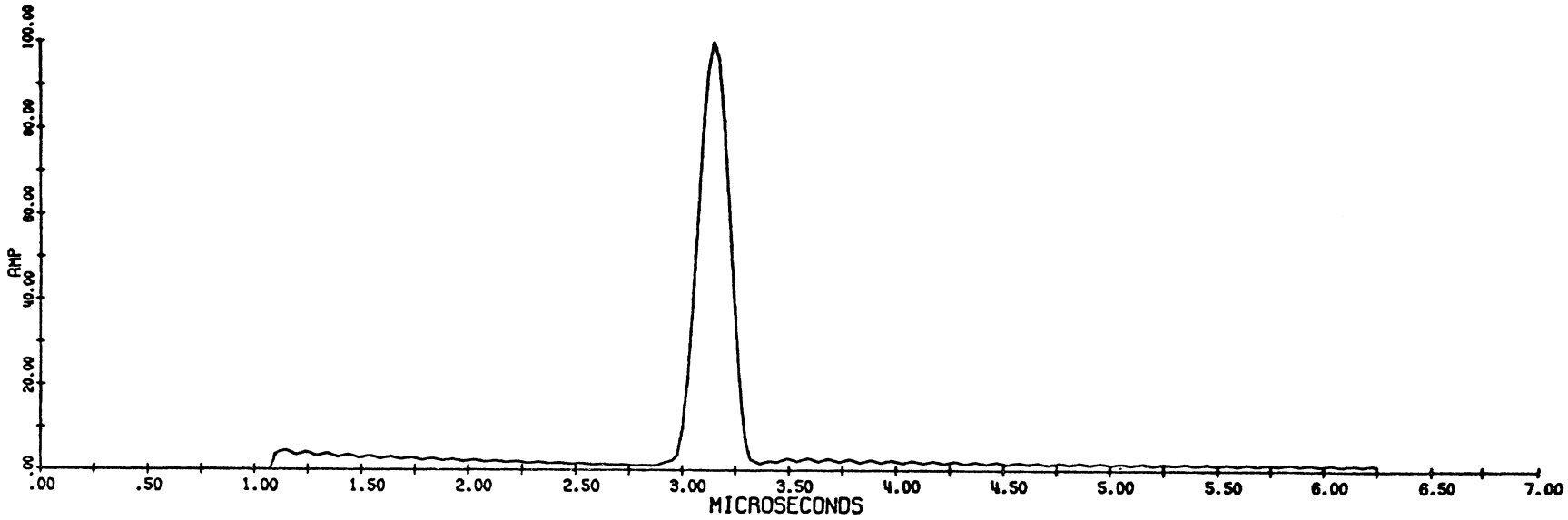

Figure 24. Computer simulation of the effect of scattering on a single target with $d_1 - d = +127$ mm.

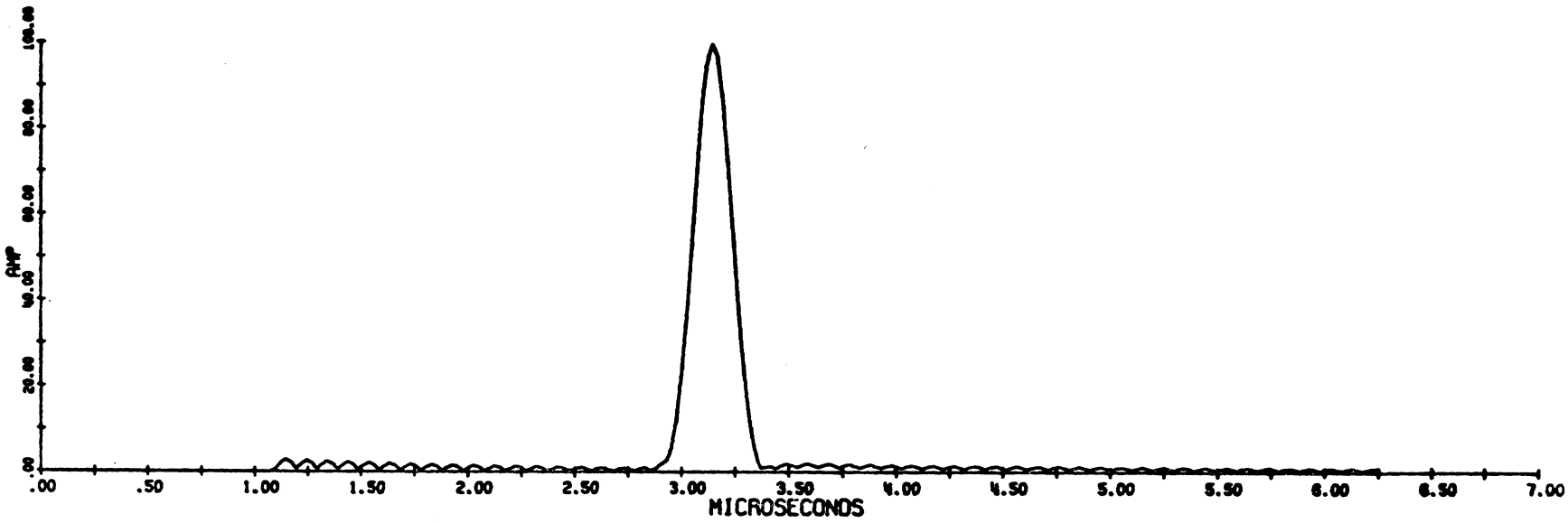

Figure 25. Computer simulation of the effect of scattering on a single target. $M(f) = \exp(\eta f^2)$.

and the reference function. As Figures 20-25 show, uncompensated scattering lowers the maximum SNR but maintains the full resolution capability of the system.

In order to calculate $M_2(f)$, it is necessary to determine B_1, and B_2. Mason (1950, page 419) presents some experimental data for aluminum with an average grain size of 0.23 mm that is well-fitted by the following values of B_1 and B_2.

$$B_1 = 8.86 \times 10^{-3} \text{ dB/mm/MHz}$$

$$B_2 = 3.94 \times 10^{-5} \text{ dB/mm/MHz} \qquad (33)$$

Once $M_2(f)$ is known, then equation 58 is used to find the final output function, $S(f)$. The effect of the scattering medium can be best illustrated by using a single point target, in which case $G(f) = 1$ and

$$S(f) = M_2^2(f) + M_2(f) \cos(2\pi fT) + 1 \qquad (34)$$

$S(f)$ is calculated for various values of $d_1 - d$ over a frequency range approximately the same as the bandwidth of the transducer used in Figure 12. It is then multiplied by a Hamming window function and inverse Fourier transformed to yield the results shown in Figures 20-24. When $d_1 - d$ is negative, the simulated discontinuity precedes the reference function. When $d_1 - d$ is positive, the reference function precedes the simulated discontinuity. For all the data presented in Figures 9-18, $d_1 - d$ is negative. For comparison purposes, the target position on the time axis is the same for each figure even though $d_1 - d$ varies from figure to figure.

The result of applying this analysis to the case of simulated single point target is that there is a neglible difference in resolution as a function of scattering. The main effect of the scattering is to reduce the maximum SNR.

APPLICATIONS

Figures 9-18 demonstrate that processing the data returned from an ultrasonic pulse-echo system in the manner described in Section II can increase the resolution, increase the SNR, and rpovide an output display that is independent of any particular transducer. These three improvements can be used to increase the information presented in the following ultrasonic NDT situations

The increased resolution can distinguish between a rough, extended defect and porosity. Using the old, low resolution systems, both the porosity and the extended defect have the same display indications. As the resolution increases, the rough surface shows many closely spaced targets with no gaps, while the porosity shows discrete targets separated by distinct gaps. Thus, the appearance of gaps can be used to indicate porosity in a high resolution system.

The increased resolution can also identify defects which are located very close to a known surface. In a conventional, low resolution system, the strong echo from the known surface masks the weak echoes from small targets located nearby. As the resolution increases, the region over which this masking occurs diminishes.

High resolution is also potentially important in the testing of spot welds in thin plates. Existing techniques, both through-transmission and pulse-echo, rely on the premise that such undesirable factors as low penetration, porosity, expulsion, and an undersized nugget cause variations in attenuation. While this premise is true, such tests do not identify the particular type of defect, nor do they locate the position of the defect within the weld. A high resolution pulse-echo system has the capability of locating such defects as expulsion and porosity, and if the acoustic impedance of the fused material is sufficiently different from the parent material, it can measure penetration and nugget size as well.

As mentioned in the last part of Section I, this data processing scheme is intended to be used as part of a scanning system that will display an outline of the defect. In such a system, high resolution is very important since the determination of the strength of a material containing a discontinuity is dependent on the orientation of the discontinuity and whether it is large or small, smooth or rough, spherical or crack-like, etc.

A schematic diagram of a one-dimensional scanning system is shown in Figure 26. The transducer is placed in position A, and data are collected and stored exactly as for the data in Figures 8-17. The transducer is then placed in positions B, C, D, etc., and the data are collected and processed as in position A. After the scan has been completed, a high resolution (both lateral and longitudinal) "A" scan for position C, for example, can be formed by point-by-point addition of the data from positions A-E. The computer addition of the data from positions A-E simulates the physical addition of the signal that would occur in a single transducer whose diameter is equal to the length of the line segment AE. Thus, high lateral resolution is achieved by computer addition, and high longitudinal resolution is achieved by computer deconvolution.

The lateral resolution can be further increased by the addition of more positions, as long as the transducer beamwidth is adequate to insonify the

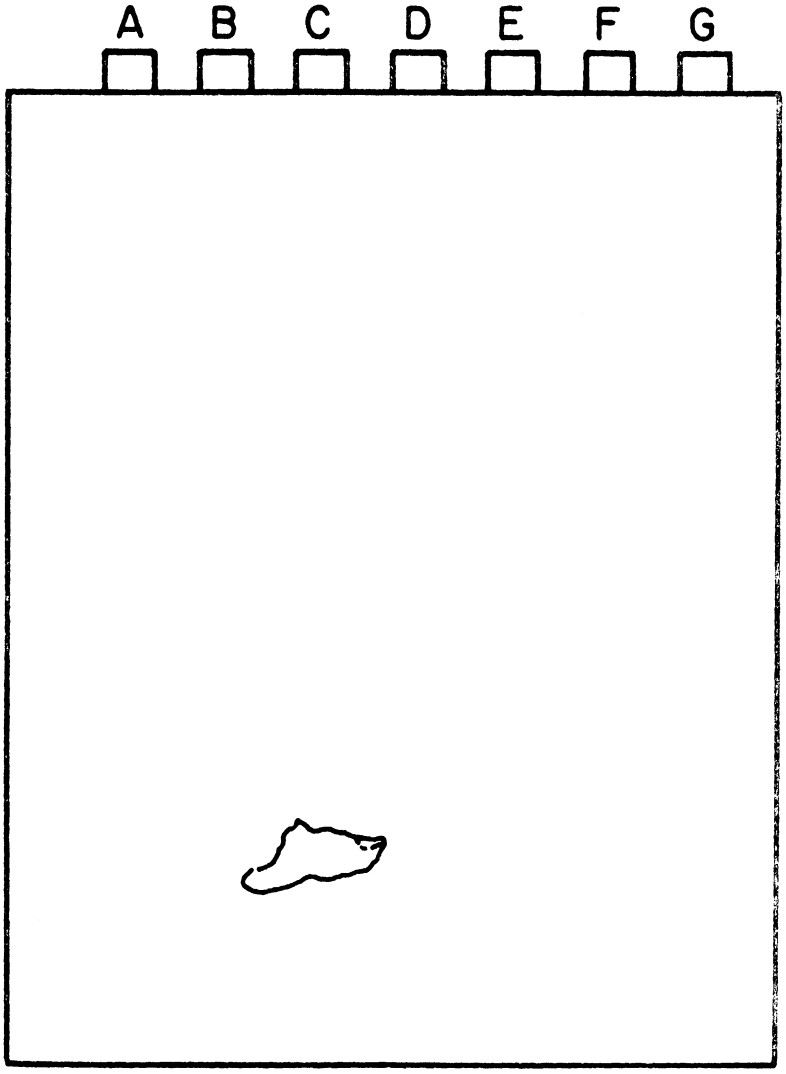

Figure 26. Schematic diagram of a phased array scanning system. Points A through G represent the same transducer at various positions during the scan.

target. This fact has the interesting consequences that the lateral resolution is increased by using a smaller diameter transducer, and that the resolution of the processed data will be independent of the target range. Since the transducer beamwidth is inversely proportional to its diameter, a small transducer will have a large beamwidth. If the target is located directly under position C, a large beamwidth transducer will allow positions D, E, F, etc., to insonify and to collect data from this target, and the more positions that insonify a given target, the higher the lateral resolution. The range-independent resolution is due to the fact that the resolving power is directly proportional to the equivalent transducer diameter and inversely proportional to the range while the equivalent transducer diameter is directly proportional to the range. Thus the range term cancels out.

From just this short description of a possible scanning system, it can be seen that it has many inherent advantages over the conventional amplitude comparison technique of defect characterization. Besides having advantageous characteristics of its own, the data processing system that has been described produces data in a form ideally suited for the realization of this scanning technique. As equation (12) in Section II shows, the data processing output contains both the amplitude and phase information present in the reflectivity function. Without both amplitude and phase information, it is impossible to achieve the full benefits of the scanning system.

The SNR improvement offered by the data processing system is also an important part of the proposed scanning system. Since small diameter transducers will be used in order to increase the lateral resolution of the scanning system. The unprocessed SNR at any given position in Figure 26 will be decreased accordingly. The signal averaging implemented by the data processing system increases the SNR before the array processing and prevents the small diameter transducer from adversely affecting the final SNR. The array processing used in the scanning system also decreases the noise due to the random grain structure. Again, this noise is decreased by the signal averaging performed during the addition of the data from the many different transducer positions.

The SNR improvement demonstrated in Figure 17 can be very important in the application of ultrasonic NDT to such materials as titanium billets and centrifugally-cast pipes. As Sattler (1969) shows, the SNR of a conventional pulse-echo system used to test titanium billets is very low. He states that "A" 10-MHz test frequency proved unfeasible because of high attenuation and low signal return." Using the data processing system, the SNR could be improved enough to enable the testing to proceed at the 10-MHz frequency. Without data processing, the tests would have to be performed at lower frequencies with an attendant loss in resolution. In the case of centrifugally-cast pipe, the microstructure is very large and preferentially oriented along the lines of force present during the casting process. This microstructure scatters a large proportion of the ultrasonic energy and makes it practically impossible to use conventional ultrasonic NDT. The SNR improvement demonstrated in

Figure 17 opens up the possibility that defects that are large with respect to the microstructure may be located by ultrasonic techniques even in centrifugally-cast structures.

The third advantageous characteristic of the data processing system, transducer independence, makes display interpretation very easy. Since the ringing response of the transducer is completely removed, the processed display has all the advantages of a rectified and filtered display. A single target is represented by a single, unipolar indication. The display is also independent of normal transducer aging and replacement. This feature is very important when test results are compared for change over a period of years. In a conventional system, the transducer may age or need to be replaced, and when the new test data are compared to the old, apparent changes may be due to the different transducer rather than to discontinuity growth. If the data from both the new and the old tests are deconvolved, the effect of the transducer on the test is negligible and any changes in test data can be confidently attributed to discontinuity growth.

This data processing system can also be applied to shear wave and surface wave testing. The SNR enhancement and frequency dependent media compensation are especially important properties for use in shear wave systems since the lower velocity of shear waves produces a smaller wavelength that is more easily scattered and attenuated by the material microstructure.

The application of this processing scheme to "pitch-catch" and through-transmission systems that use two transducers is limited by the complexity of the necessary deconvolution filter; no simple amplitude-only filter can be formed. The SNR enhancement procedure could be applied separately, in such cases, without any deconvolution, if it is necessary to improve the sensitivity of the system. But this approach should be considered only after rejecting any alternative techniques.

VI. CONCLUSIONS

A new approach to ultrasonic pulse-echo NDT has been presented. It utilizes computer data processing of the information in the echo in conjunction with a computerized scanning system to form a visual display containing an outline of the hidden discontinuity. At present, a large amount of ultrasonic pulse-echo NDT information is being discarded because minimal use is made of the correlation of the information returned from adjacent transducer echoes in time and from adjacent transducer positions in space. Experimental evidence has been presented to demonstrate that the information inherent in the time sequence of transducer echoes can be processed by computerized signal averaging to provide a 28 dB increase in the SNR over that available from a conventional system. This experimental evidence also demonstrates that computer processing of pulse-echo data can increase the longitudinal resolution by a factor of five and can present a display that is virtually independent of the physical characteristics of the particular transducer used to collect the data.

A mathematical model of this system provides an especially simple form (amplitude only) for the deconvolution filter used to increase the longitudinal resolution. This model also provides a formula expressing the SNR of the output in terms of the SNR of the input and the system parameters, such as the number of samples and the filter bandwidths. An analysis of this model also shows that, by the proper use of a reference function required in the data acquisition stage, the effect of frequency-dependent scattering in the medium can be partially removed. A computer simulation, designed to show the remaining residual effect of frequency-dependent scattering in the medium demonstrates that the uncompensated scattering causes a negligible decrease in the resolution and a slight decrease in the maximum SNR.

Due to the presence of high frequency information in the raw data, digital data cannot be acquired directly from the ultrasonic echo. To circumvent this problem, a data acquisition system which utilizes a holographic approach preserving both the amplitude and the phase information present in the ultrasonic echo is developed. Since the digital data preserves both the phase and amplitude of the ultrasonic echo, it can be stored and then recombined at the completion of a scanning procedure to form a synthetic array of transducers. Such an array processor should increase the lateral resolution of the transducer and increase the SNR for noise generated by the material microstructure in the neighborhood of the defect target.

The application of this data processing system to current problems in ultrasonic pulse-echo NDT is also discussed. When applied to immersion testing, the system is capable of revealing discontinuities lying closer to the front surface of a part than can be detected with a conventional system. The

improved resolution makes it easier to differentiate between porosity and a large extended defect. The transducer-independent visual display is able to compare test results taken over a time period in which it is possible that the transducer may have aged or been replaced. And finally, the improved SNR increases the sensitivities of ultrasonic pulse-echo testing in materials such as cast titanium and to centrifugally cast pipe where the grain structure causes excessive scattering of the ultrasonic pulse.

VII. FUTURE WORK

The next logical step in the development of this data processing system is to construct an array processor. Initially, a few simple targets could be scanned from a plane surface, and the data from each transducer position could be summed and displayed in order to establish the lateral resolution. At this stage, close attention should be paid to the effect of the contact conditions between the transducer and the test sample. After this experiment, the scanning system can be generalized to surfaces with arbitrary curvature and to complex targets.

The data acquisition system used in this research was necessary in order to accurately measure and record the high frequency data in the ultrasonic echo. If sample-and-hold modules with aperture times on the order of 0.5 ns or less become available, then a much simpler and cheaper data acquisition system is possible. Recent developments in commercial sample-and-hold modules indicate the possibility of such high speed units. In this case, the data would be collected directly from the ultrasonic echo and no reference function would be necessary. If the testing material has little attenuation, a single deconvolution filter can be constructed and applied to all the data. If the material is highly attenuating, then a different filter can be constructed for each distance interval, and in this manner, the effects due to scattering and attenuation can be minimized. The latter possibility, while a little more complex than the former, is scarcely more time consuming when implemented on a digital minicomputer.

For the purposes of this research all the digital data processing was done on a large, central computer. The necessary processing, though, is quite simple, and commercially available minicomputers with 8K storage are capable of handling the necessary data acquisition and processing. A system designed around such a minicomputer could be made portable with no loss of performance and a large gain in convenience.

And finally, with the development of an array processor, the problem of information display must be considered. "A" scan, "B" scan, and "C" scan displays can all be formed by the array processor, but there are many advantages to be gained by considering cross-sectional and isometric projection displays. A display, or displays, should be chosen to optimize the human interpretation of such large amounts of data.

REFERENCES

Cox, C. W. and Renken, C. J., 1970. "The application of signal-processing techniques to signals from electromagnetic test systems." Materials Evaluation, Vol. 28, No. 8, p. 173.

Davenport, W. B. and Root, W. L., 1958. Random Signals and Noise, McGraw-Hill Book Company, Inc., New York.

Gold, B. and Rader, C. M., 1969. Digital Processing of Signals, McGraw-Hill Book Company, Inc., New York.

Kaplan, W. F., 1962. Operational Methods for Linear Systems, Addison-Wesley, Inc., Reading, Massachusetts.

Mason, W. P., 1950. Piezoelectric Crystals and Their Application to Ultrasonics, D. Van Nostrand and Company, New York.

Sattler, F. J., 1969. "Nondestructive testing techniques for titanium billets." Technical Report AFML-TR-68-345, TRW, Inc., Cleveland, Ohio.

Serabian, S., 1968. "Implications of the attenuation-produced pulse distortion upon the ultrasonic method of nondestructive testing." Materials Evaluation, Vol. 26, No. 9, p. 174.

Seydel, James A., 1972. Computerized Enhancement of Ultrasonic Nondestructive Testing Data. Ph.D. Thesis, The University of Michigan (1972).

Sokolov, S. J., 1941. "Ultrasonic methods for determining the properties of heat-treated steel and for determining internal flaws of metal objects." Zhurnal Tekhnicheskoi Fiziki (printed in Russian), Vol. 11, p. 160.